EURADOS Report 2020-05
Neuherberg, October 2020

EURADOS
European Radiation Dosimetry Group e. V.

A model validation scheme for Monte Carlo simulations of a medical linear accelerator: geometrical description and dosimetric data used in the "Linac Action"

Barbara Caccia, Valentin Blideanu, Maïwenn Le Roy, Hans Rabus, Rick Tanner

ISSN 2226-8057
ISBN 978-3-943701-24-1

European Radiation Dosimetry Group e.V.

EURADOS Report 2020-05

Neuherberg, October 2020

A model validation scheme for Monte Carlo simulations of a medical linear accelerator: geometrical description and dosimetric data used in the "Linac Action"

Barbara Caccia[1], Valentin Blideanu[2], Maïwenn Le Roy[2], Hans Rabus[3], Rick Tanner[4]

[1] Istituto Superiore di Sanità (ISS), Rome, Italy

[2] Institut LIST-Laboratoire National Henri Becquerel (LNE-LNHB), CEA, Université Paris-Saclay, Palaiseau, France

[3] Physikalisch-Technische Bundesanstalt (PTB), Berlin, Germany

[4] Public Health England, Chilton, Didcot, United Kingdom

ISSN 2226-8057

ISBN 978-3-943701-24-1

Imprint

Issued by:
European Radiation Dosimetry e. V.
Postfach 1129
85758 Neuherberg
Germany
office@eurados.org
www.eurados.org

The European Radiation Dosimetry e.V. is a non-profit organization promoting research and development and European cooperation in the field of the dosimetry of ionizing radiation. It is registered in the Register of Associations (Amtsgericht München, registry number VR 207982) and certified to be of non-profit character (Finanzamt München, notification from 2019-10-14).

Liability Disclaimer

Members of the editorial group

This report was prepared by the following members of EURADOS Working Group 6 on "Computational Dosimetry":

Barbara Caccia	Istituto Superiore di Sanità National Center for Radiation Protection and Computational Physics 00161 Rome, Italy
Valentin Blideanu	Institut LIST-Laboratoire National Henri Becquerel (LNE-LNHB), CEA, Université Paris-Saclay, 91120 Palaiseau, France
Maïwenn Le Roy	Institut LIST-Laboratoire National Henri Becquerel (LNE-LNHB), CEA, Université Paris-Saclay, 91120 Palaiseau, France
Hans Rabus	Physikalisch-Technische Bundesanstalt 10587 Berlin, Germany
Rick Tanner	Public Health England Chemical & Environmental Hazards, Centre for Radiation Didcot OX11 0RQ, United Kingdom

List of contributors to the report

Jean-Marc Bordy	Institut LIST-Laboratoire National Henri Becquerel (LNE-LNHB), CEA, Université Paris-Saclay, F-91120, Palaiseau, France
Valentin Blideanu	Institut LIST-Laboratoire National Henri Becquerel (LNE-LNHB), CEA, Université Paris-Saclay, F-91120, Palaiseau, France
Barbara Caccia	Istituto Superiore di Sanità, National Center for Radiation Protection and Computational Physics 00161 Rome, Italy
Loïc de Carlan	DES-Service d'études des réacteurs et de mathématiques appliquées (SERMA), CEA, Université Paris-Saclay, 91191 Gif-sur-Yvette, France
Maïwenn Le Roy	Institut LIST-Laboratoire National Henri Becquerel (LNE-LNHB), CEA, Université Paris-Saclay, 91120 Palaiseau, France
Robert Price	Inrad-Medical Market Drayton TF9 4HX, United Kingdom
Hans Rabus	Physikalisch-Technische Bundesanstalt 10587 Berlin, Germany
Rick Tanner	Public Health England Chemical & Environmental Hazards, Centre for Radiation Didcot OX11 0RQ, United Kingdom

Content

Abstract

Radiation therapy has become more complex over the past few years with the use of new techniques like IMRT (Intensity Modulated Radiation Therapy) and stereotactic treatments. Moreover, optimisation of the radiotherapeutic treatment has become a critical point in the overall planning and delivery process due to the trend in dose-escalation with these new techniques and the associated risk for damage to healthy tissue. Typically, in techniques such as IMRT the dose distribution includes steep dose gradients with complex concave patterns. In order to calculate such complex three-dimensional distributions and deliver the proper dose to the tumour, the treatment planning system (TPS) has to perform complex calculations (usually in a short time) based on various approximations to the radiation transport process. Monte Carlo (MC) simulations can be beneficial in such circumstances – either as a means of undertaking the whole calculation (although this is still not often used in practice) or for validating the results achieved with a commercial TPS (Rogers 2006). Moreover, MC calculations are commonly used in the establishment of the primary standards for calculation of correction factors not accessible to experimental determination.

Working Group 6 (WG6) of EURADOS is dealing with various aspects of computational dosimetry in medical applications. The aim of WG6 is promoting good practice in the field of computational methods in radiation dosimetry for radiation protection and applications in radiation medicine.

WG6 has been organizing intercomparisons on computational dosimetry for many years. In 2010 an intercomparison exercise was proposed with the aim of comparing the results obtained when different users apply different MC models to simulate a medical linear accelerator (LINAC), with approaches differing according to the MC code used and other parameters, such as the initial electron beam parameters and voxel size. This exercise has been called "Linac Action" and focused on the characterization of the therapeutic beam and on the calculation of the dose distributions in water phantoms and in several heterogeneous phantoms for a nominal 12-MV photon beam (Caccia *et al.* 2017).

The goal of the Linac Action was to monitor the state of the art regarding MC approaches for characterizing medical LINACs and to provide a learning-by-doing self-training exercise that supports MC users in developing the skills needed to (a) set up and calibrate a MC simulation of a real linear accelerator and (b) perform a dosimetric analysis by comparing their results with measured reference data. The aim of this report is to provide the experimental data needed and a description of the MC modelling for those who want to start a Monte Carlo modelling activity in the field of oncological radiotherapy. Therefore, this report gives a compilation of the data needed for simulating the linear accelerator considered in the exercise and for evaluating the dose distribution obtained with such a MC simulation by comparing it with the measured dosimetric data used in the intercomparison exercise.

1. Task outline

The report provides dosimetric data and descriptive elements of a linear accelerator (LINAC) that allow the development of a Monte Carlo simulation model of a well characterized medical linear accelerator used for primary measurements. This standard model can be used to help users develop the skills needed to build and calibrate a Monte Carlo simulation and perform a dosimetric analysis. The implementation of the Monte Carlo model of this dosimetric system is divided into two tasks (Task 1 and Task 2) that must be performed in succession.

1.1 Task1: to model the head of the LINAC

The first task is to model the head of the GE Saturn 43 LINAC operated at CEA LIST Laboratoire National Henri Becquerel (LNHB). All relevant geometry and material data are provided, whereas the electron source information is limited. The information provided is thus typical of that normally obtainable from LINAC manufacturers and, therefore, provides a realistic scenario. Once the model geometry is constructed, the parameters related to the electron beam must be chosen, i.e. the spot size, shape, intensity profile and energy distribution, in order to be able to perform simulations of the photon field produced by the LINAC. The choice of optimal parameters should be made by comparing the simulated data calculated in a homogeneous water phantom (40x40x40 cm^3) with the experimental data provided within the LINAC Action by LNHB. These data were obtained with the LINAC set up for a single 12 MV photon field under standard reference conditions, i.e. a field size of 10x10 cm^2 field at 100 cm from the source, at 10 cm depth in water.

For those unfamiliar with this type of simulation, the procedure for adjusting the energy and spot size of the incident electrons is based on the calculation of the Percentage Depth Dose (PDD) curve and the lateral beam profiles. First, the primary energy of the incident electrons is set according to manufacturer specifications. This energy is tuned until the calculated PDD corresponds to the measured one. Second, with this energy, the spot size of the incident electron beam is changed until the calculated lateral beam profiles match the measured profiles. For the PDD curve, care must be taken to match the build-up region.

The "quality index" of the parameterization proposed in this report is based on the gamma index, which is one of the most widely used ways to assess the adherence between the simulated data and the experimental data set (Depuydt *et al.* 2002). The experimental depth-dose curve and lateral beam profile needed for model calibration are given in Annex 1. Once the electron beam parameters have been established, an MC simulation of the LINAC photon source can be performed to generate a Phase Space File (PSF) of the emitted photons for use in the second Task of the simulation model implementation.

1.2 Task2: to calculate the relative absorbed dose in dosimetric phantoms

The second task is based on the LINAC model implemented and verified in the first task. It is dedicated to calculating the relative absorbed dose in different dosimetric phantoms. With the data, both geometric and dosimetric, provided in this report a user can compare the data from their own simulation with experimental measurements for a water phantom that includes heterogeneous tissue equivalents (lung and/or bone) for 4 different configurations. The experimental data set can be used to verify whether the implemented MC model of the accelerator produces a dose distribution in dosimetric phantoms of different materials that is similar to that obtained by experimental methods.

2. Geometrical description

The linear accelerator used as a model in this report is the Saturn 43 model from General Electric (General Electric Medical Systems, Buc, France). In figure 1 there is a photo of the accelerator and a water phantom.

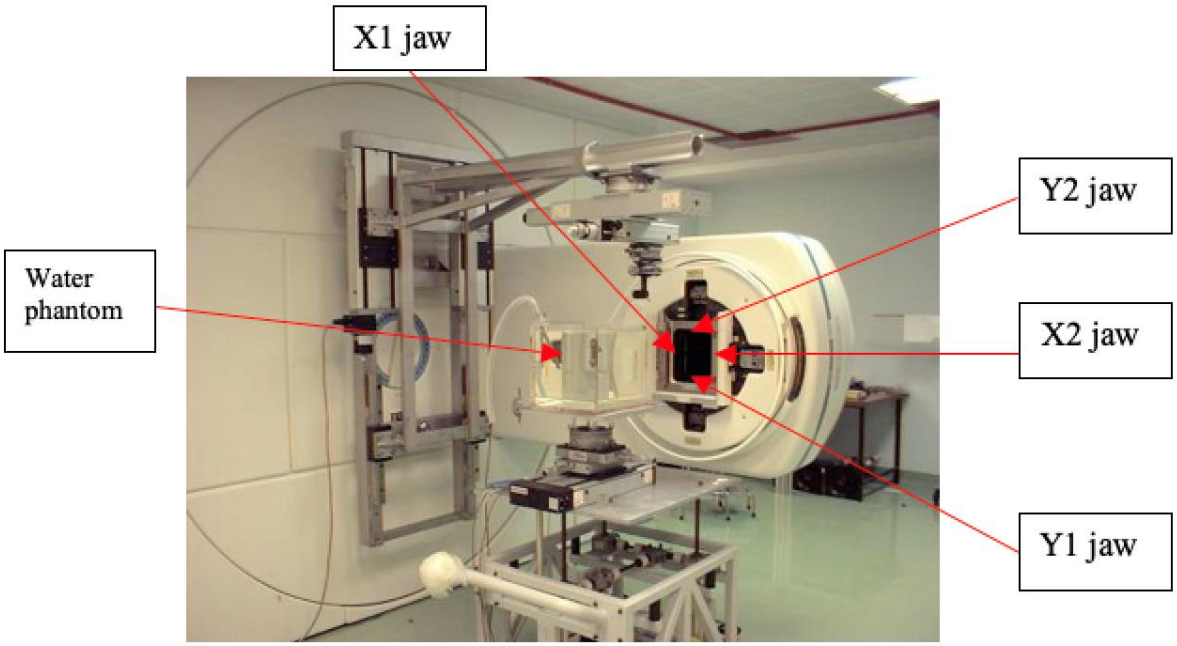

Fig. 1: A general view of the geometry of the Saturn 43 linear accelerator and the water phantom

The complete description of the geometry and materials of the LINAC is provided in the following sections. The given description of the Saturn 43 LINAC corresponds to an operational mode with an acceleration voltage of 12 MV in the photon mode with collimator settings for a 10x10 cm^2 field size at standard working distance.

2.1 Geometrical description of the LINAC head and its components

2.1.1 Field sizes

Figures 2 to 7 show schematic diagrams of the linac head indicating the positions of the adjustable beam-collimating jaws for 3 different fields (4x4, 10x10, 40x40 cm^2) in the X and Y cut. The different diagrams are not at the same scale but can be useful to have a sight of the different configuration of the LINAC head for three different irradiation fields, also if in the Linac action only the 10x10 cm^2 field was considered.

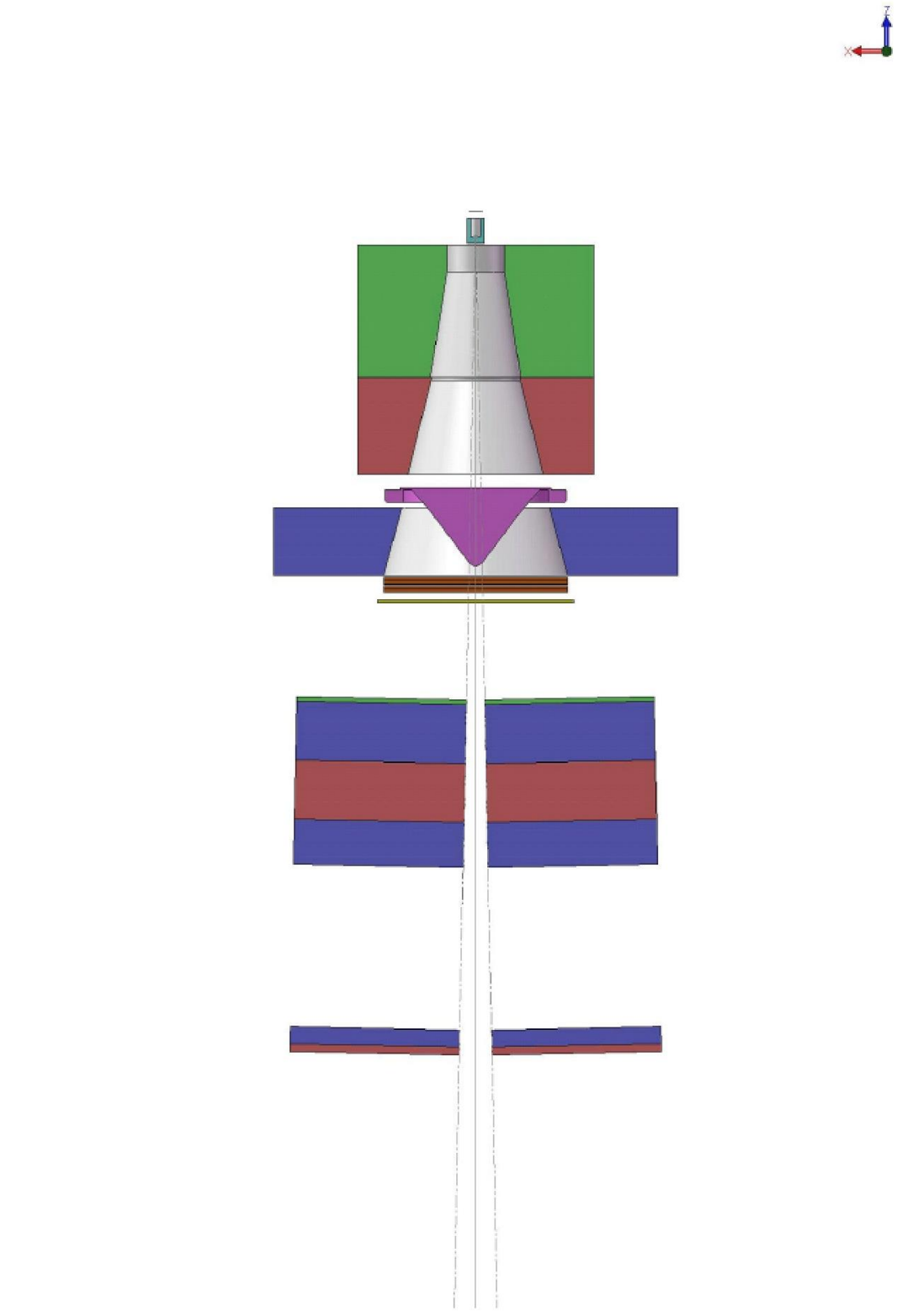

Fig. 2: Schematic side view of the Linac head illustrating the position of the collimator jaws for a 4x4 cm^2 field size at 100 cm distance from the source (X jaws view). The yaws are pivoting around an axis passing through the source point.

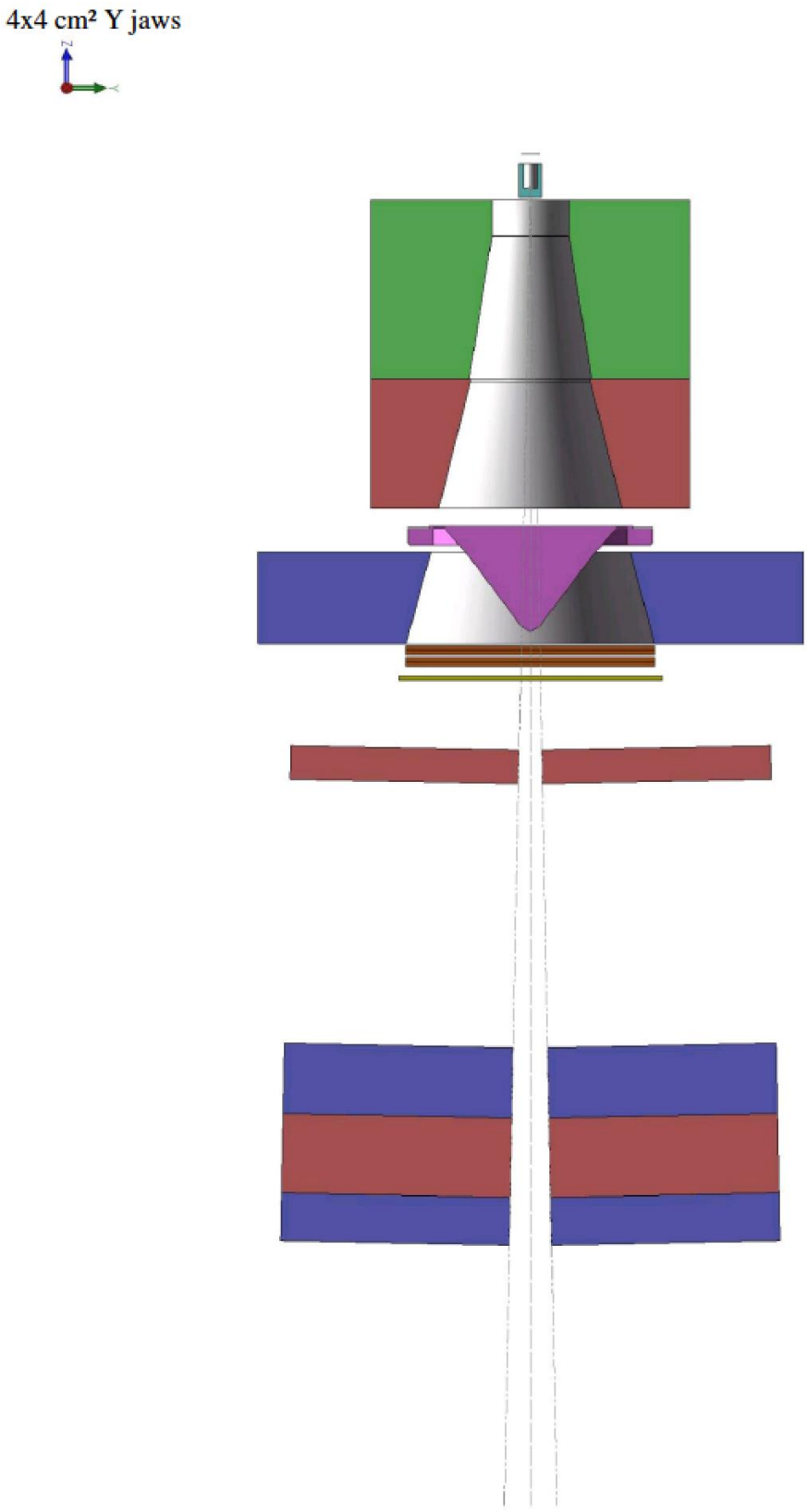

Fig. 3: Schematic side view of the Linac head illustrating the position of the collimator jaws for a 4x4 cm² field size at 100 cm distance from the source (Y jaws view). The yaws are pivoting around an axis passing through the source point.

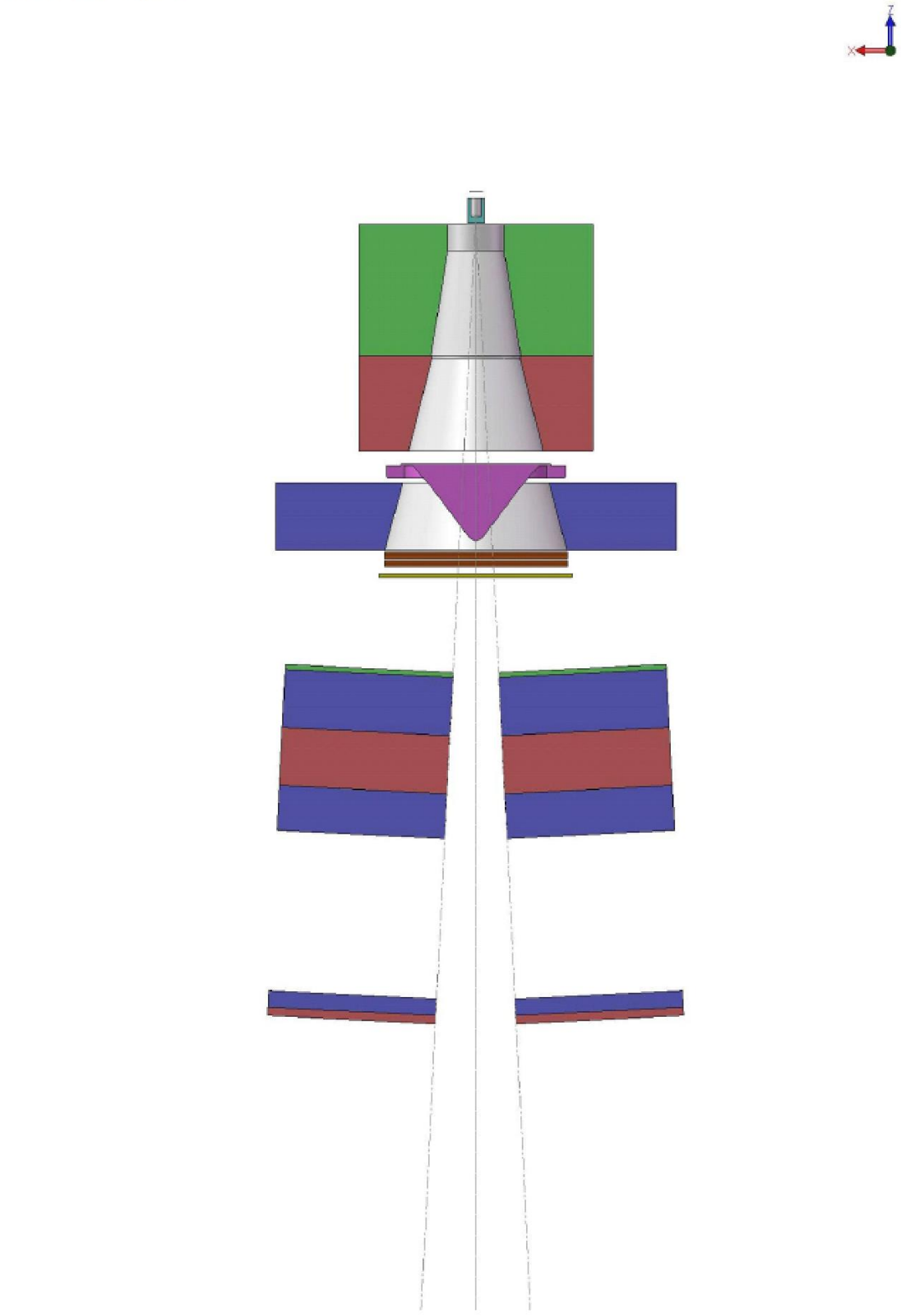

Fig. 4: Schematic side view of the Linac head illustrating the position of the collimator jaws for a 10x10 cm^2 field size at 100 cm distance from the source (X jaws view) The yaws are pivoting around an axis passing through the source point.

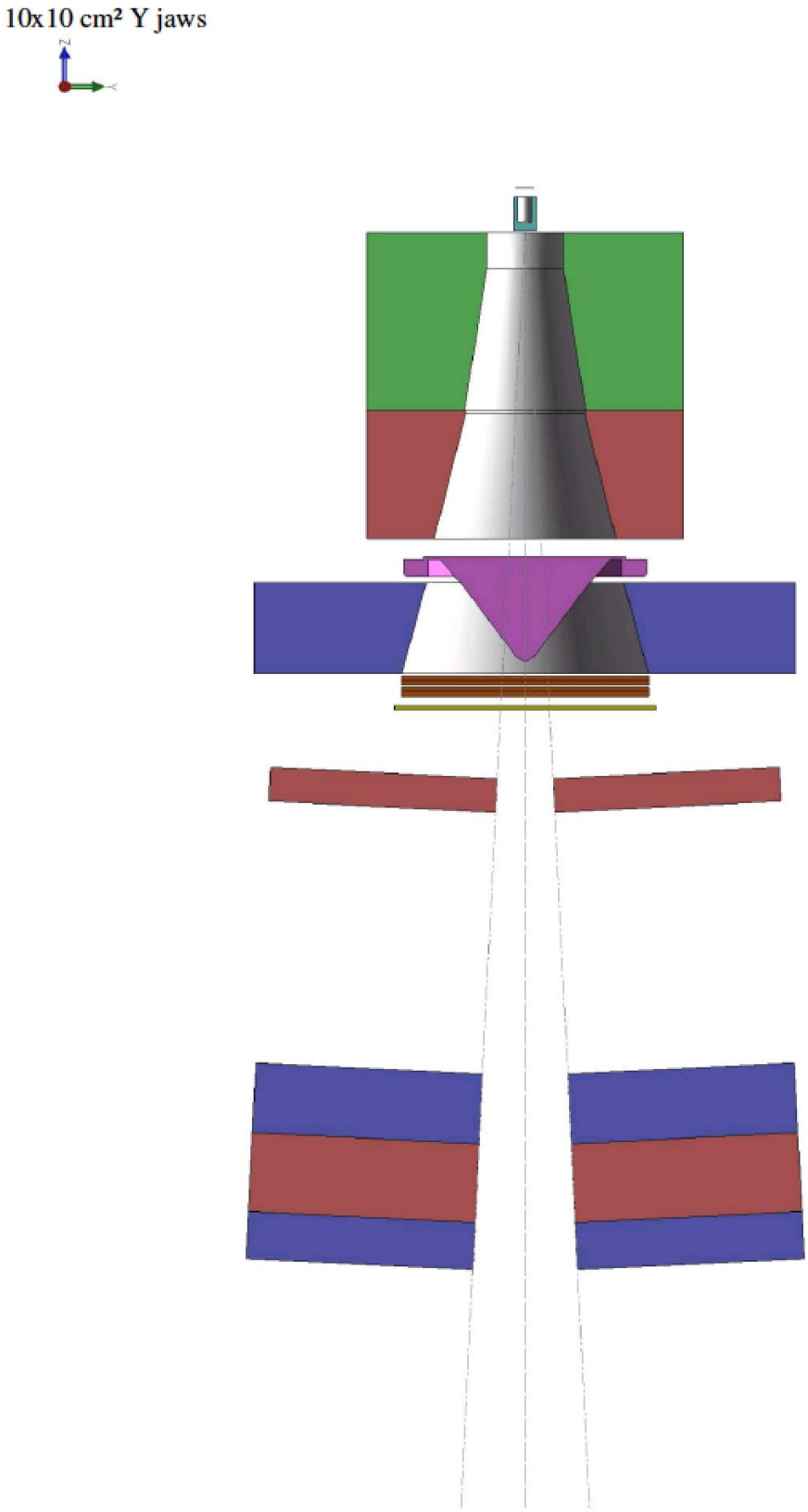

Fig. 5: Schematic side view of the Linac head illustrating the position of the collimator jaws for a 10x10 cm² field size at 100 cm distance from the source (Y jaws view). The yaws are pivoting around an axis passing through the source point.

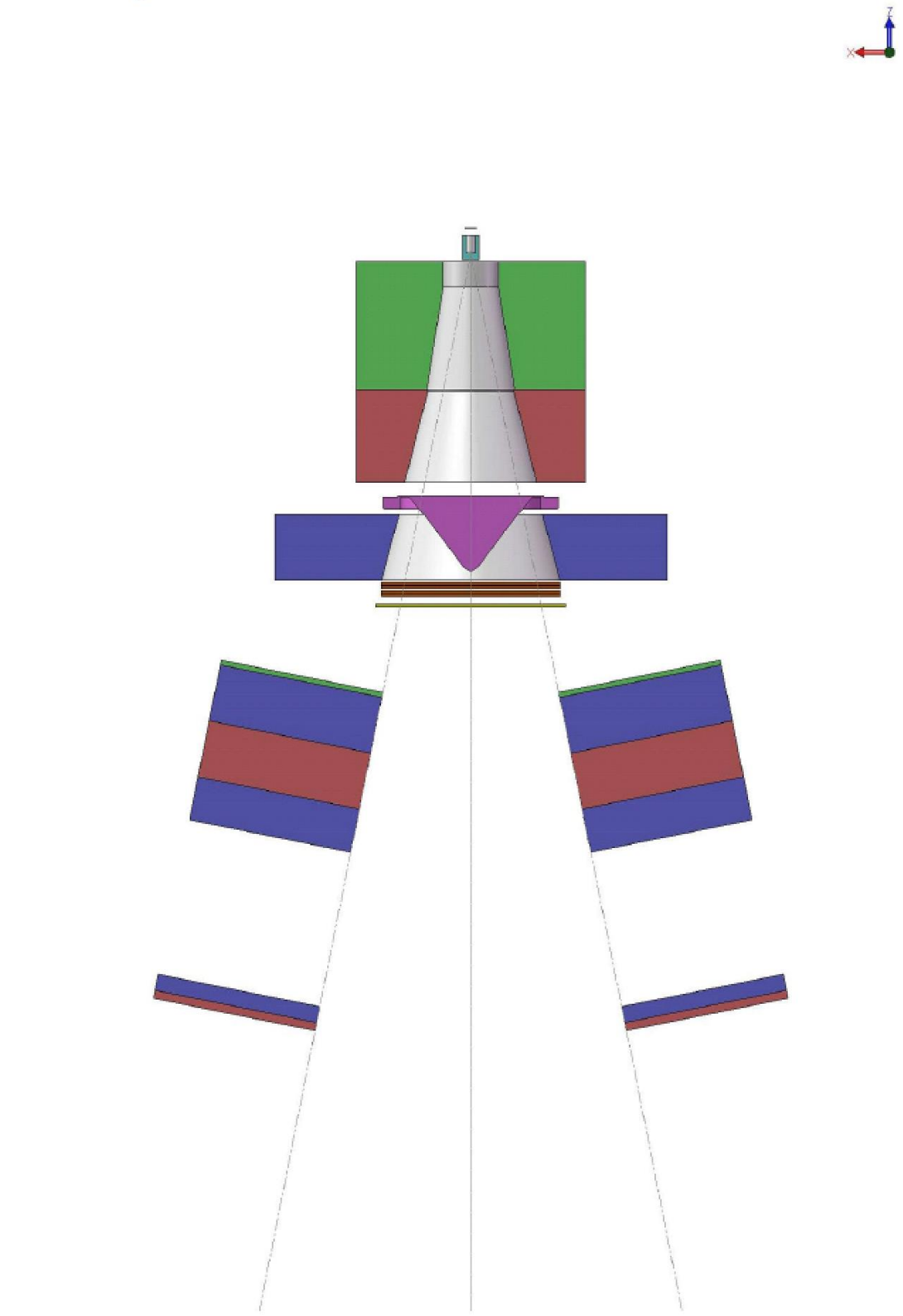

Fig. 6: Schematic side view of the Linac head illustrating the position of the collimator jaws for a 40x40 cm² field size at 100 cm distance from the source (X jaws view). The yaws are pivoting around an axis passing through the source point.

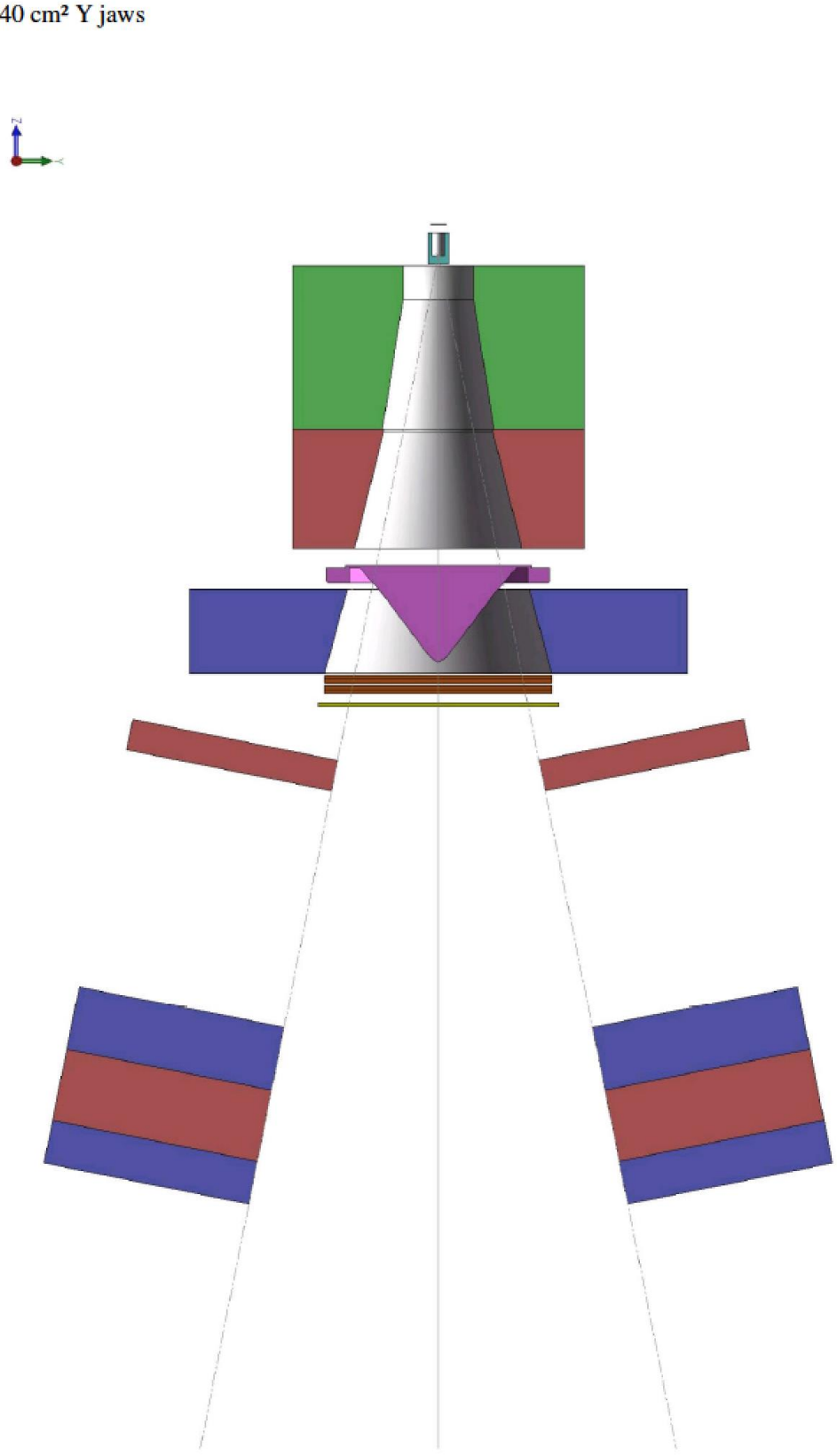

Fig. 7: Schematic side view of the Linac head illustrating the position of the collimator jaws for a 40x40 cm² field size at 100 cm distance from the source (Y jaws view). The yaws are pivoting around an axis passing through the source point.

2.1.2 Overview of Linac head geometry and material composition

Figures 8 and 9 provide the main dimensions of the linac head where in both figures the jaws are closed. Figure 8 shows a cross-sectional view in the y-z plane and gives the dimensions particularly along the beam direction. In the simulations, the origin must be considered as the point of emission of photons while the top of the titanium window is the initial point of emission of electrons for which it is requested to optimize the energy, position and any other parameter necessary for the simulation. So, the origin of the geometry is the centre of the top of the target. All surrounding material is taken to be air.

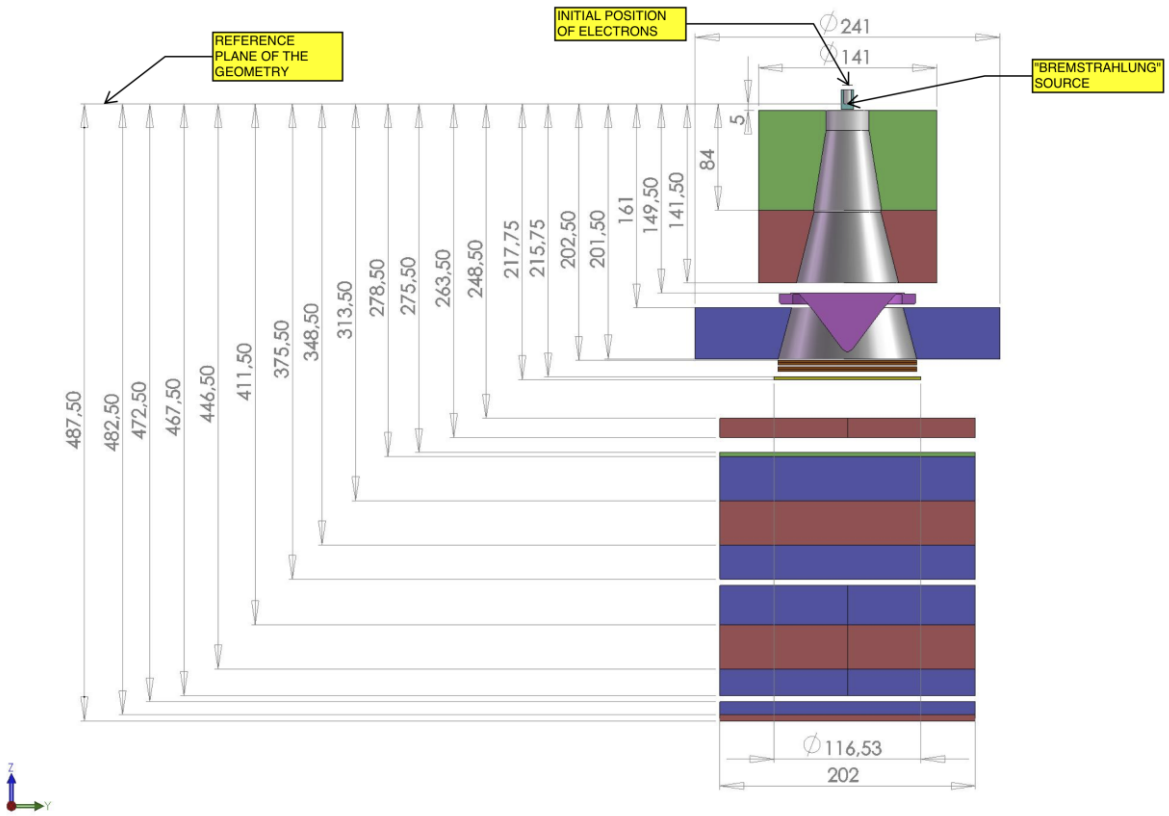

Fig. 8: Geometrical description of the head of the Linac (all dimensions in mm). With respect to the collimator yaws, the drawing corresponds to a cross section in the y-z plane. (X and Y collimator yaws have the same lateral dimensions; for thickness and material composition see Fig. 9).

Figure 9 shows a cross-section in the x-z plane and provides the thickness of all components of the head and shows the respective materials.

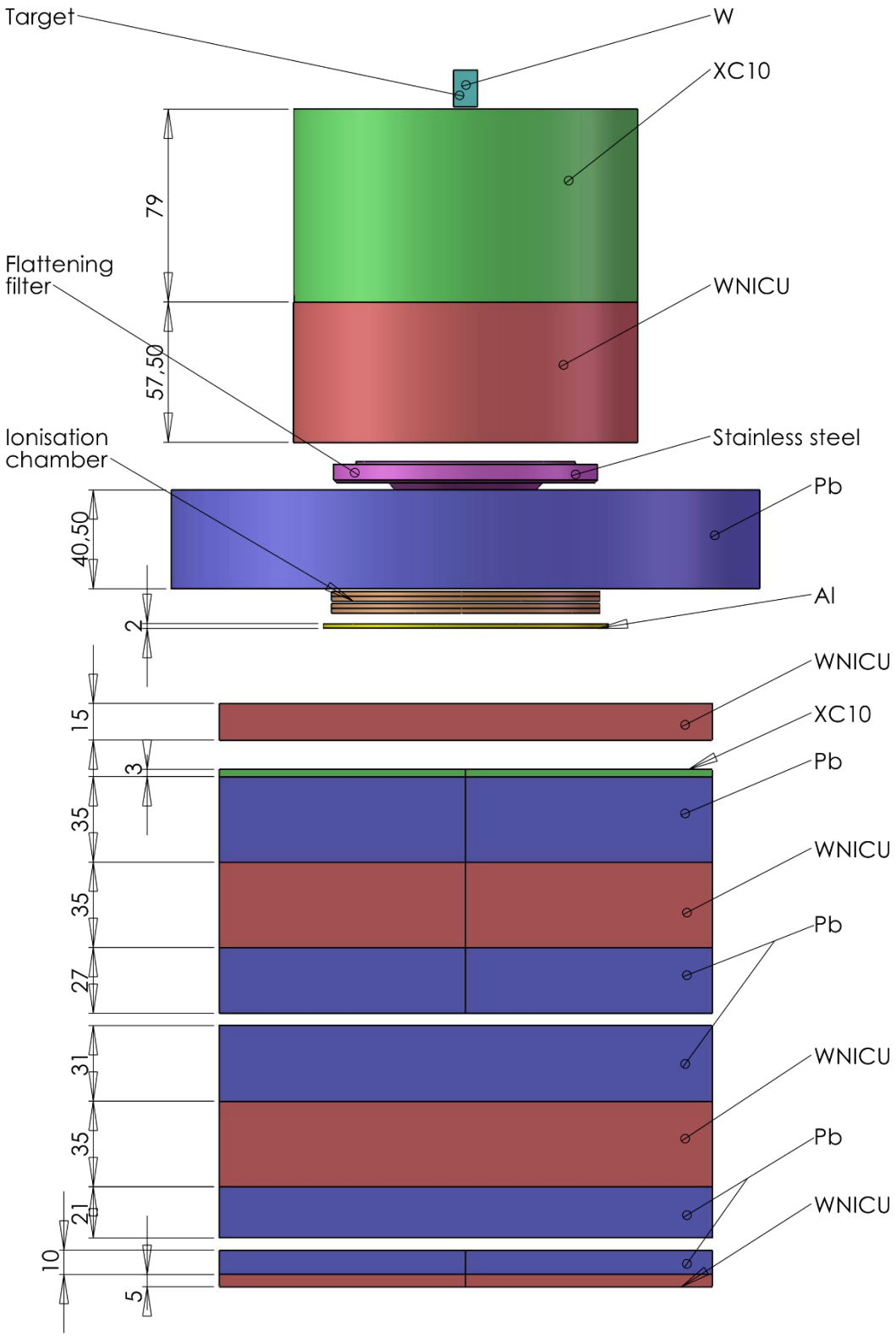

Fig. 9: Materials and thickness of the Linac components (all dimensions in mm). The drawing corresponds to a cross section in the x-z plane. Note the different thickness and material composition of X and Y collimator yaws.

2.1.3 Primary and secondary collimators

Figure 10 shows a dimensioned cross-sectional drawing of the fixed collimators (which are rotationally symmetric about the vertical axis).

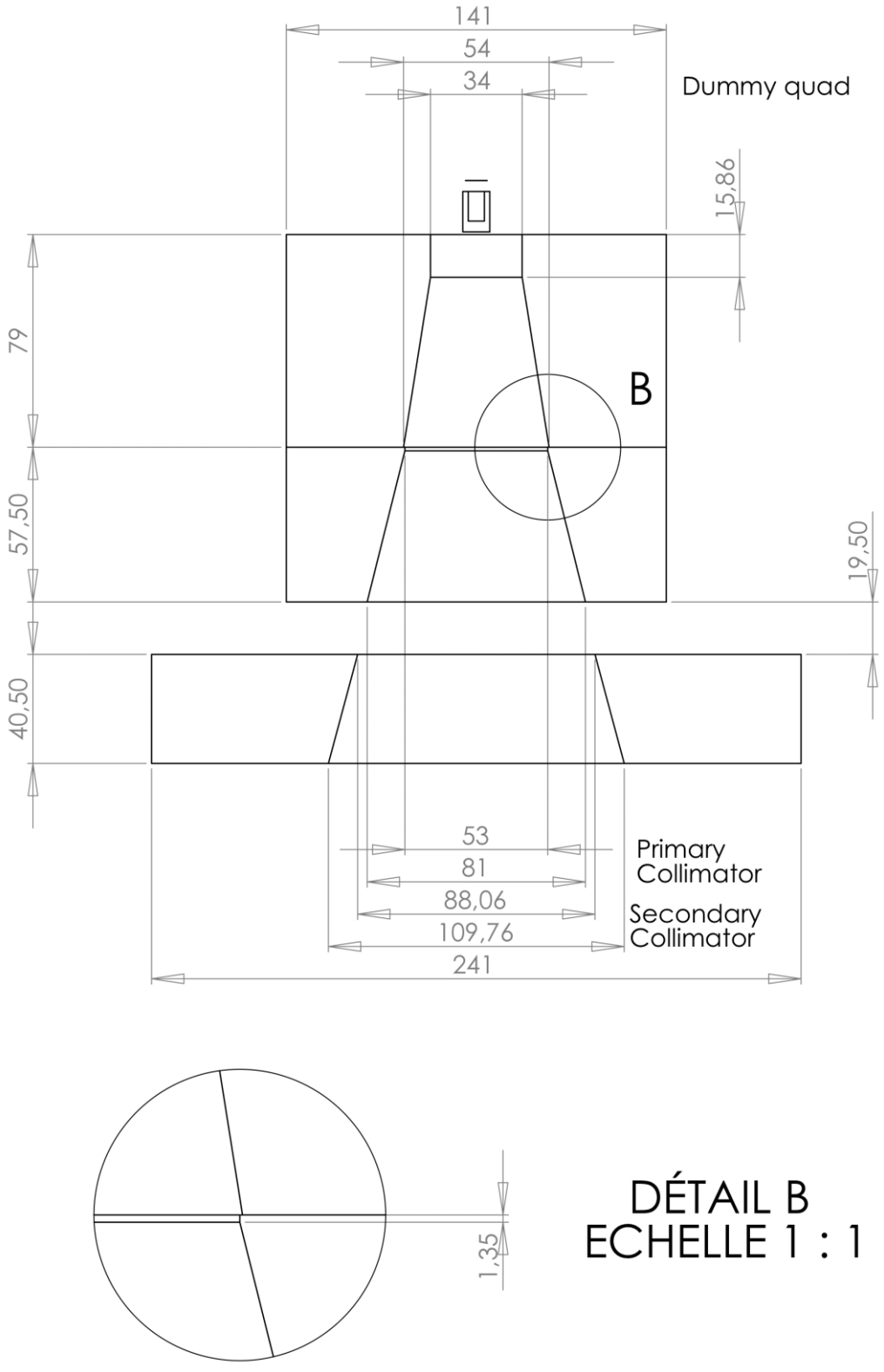

Fig. 10: Collimators: dimensions and position with respect to the source (all dimensions in mm).

2.1.4 Target

Figure 11 provides the geometrical details of the electron beam output section, consisting of the titanium window and the tungsten target.

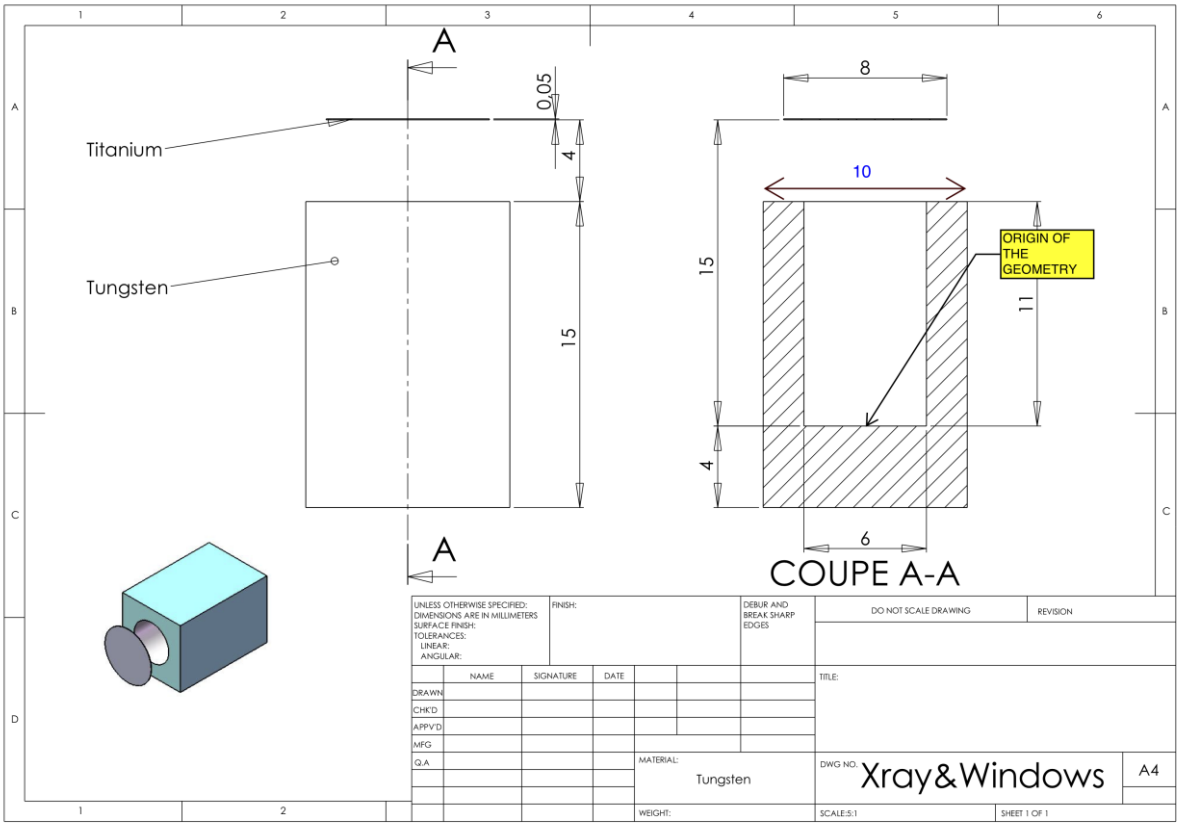

Fig. 11: Construction drawing of the target (all dimensions in mm).

2.1.5 Flattening filter

Figure 12 provides a detailed geometrical description of the flattening filter related to a photon beam produced by electrons with a nominal energy of 12 MeV.

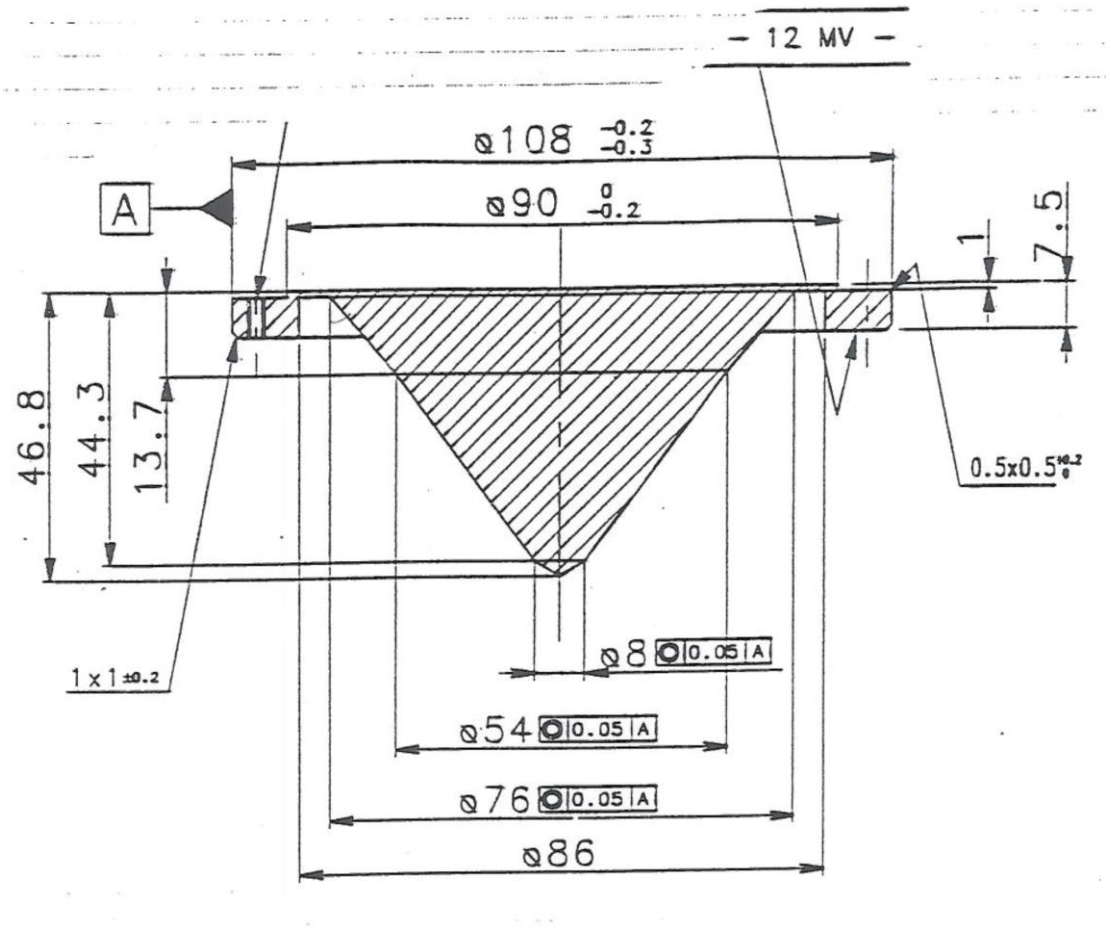

Fig. 12: Construction drawing of the flattening filter (all dimensions in mm).

2.1.6 Monitor chamber

Figure 13 provides a description of the ion chamber geometry and materials.

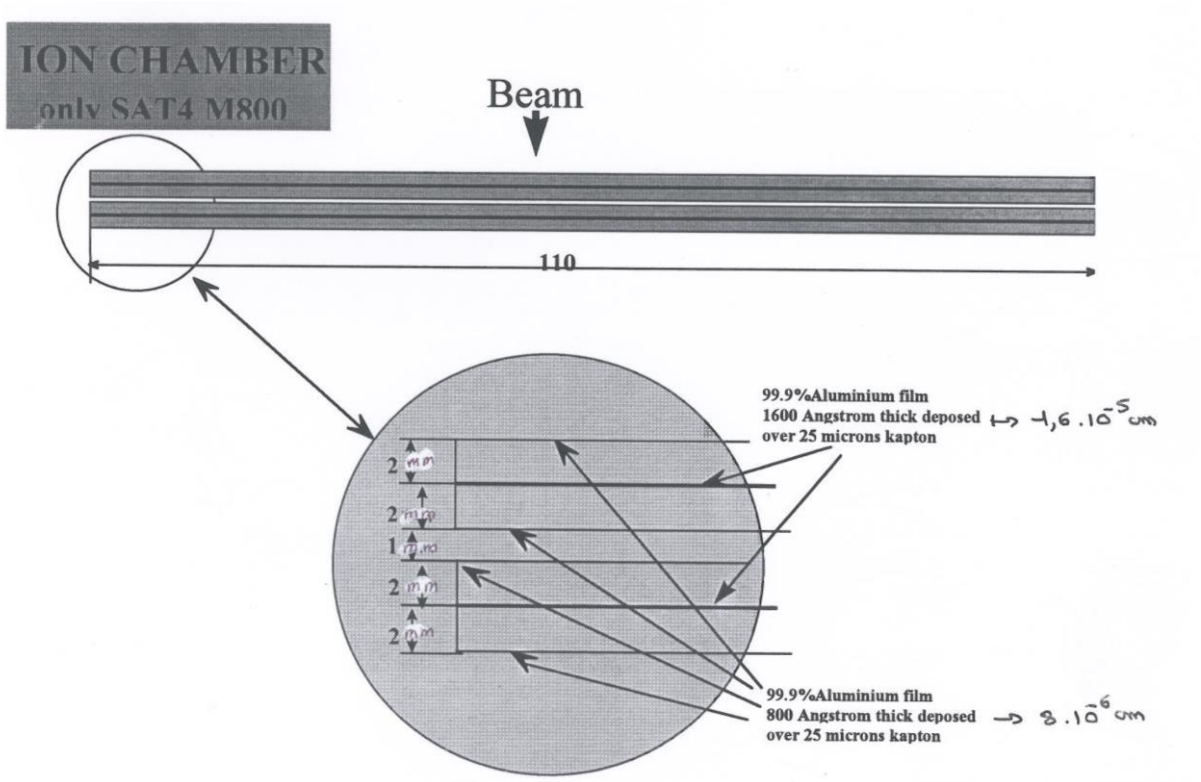

Fig. 13: Drawing of the ion chamber giving materials and geometry information. (The lateral diameter is 110 mm.

2.2 Water phantom

Figure 14 provides a detailed description of the water phantom. The water phantom consists of a 400x400x400 mm^3 polymethyl methacrylate (PMMA) water tank filled with distilled water. At the front of the phantom, the thickness of PMMA crossed by the beam is 4 mm (15 mm for the all other walls of the phantom). The distance from the source point of the target to the external entrance window of the water phantom is 90 cm. The depth in water is expressed from the external side of the entrance window of the phantom. Thus, a measurement at 10 cm depth means 4 mm of PMMA plus 9.6 cm of water. Depth in water is always expressed in cm, but for comparison of task 2 (in different heterogeneities), this depth has been converted into equivalent depth in water expressed in g/cm^2.

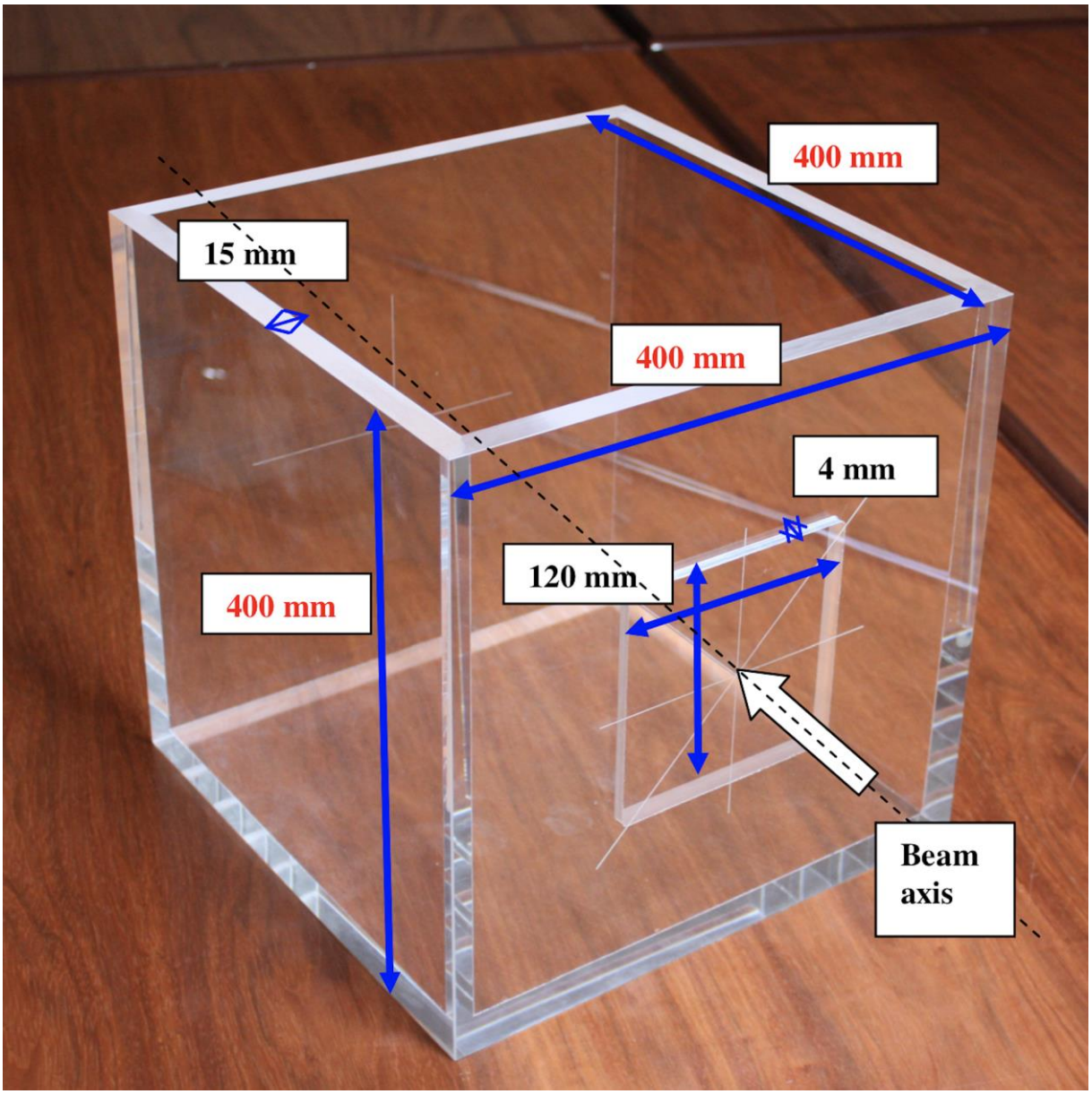

Fig. 14: Water phantom geometrical description.

2.3 List of materials

Figure 15 shows a table with the list of all the materials of the LINAC components as well as the of the dosimetric phantoms including their densities and atomic composition. The composition of each component of the materials are given in fraction by weight, expressed in %.

Table 1: Elemental composition of the materials.

	density (g.cm-3)	H 1	C 6	N 7	O 8	Mg 12	Al 13	Si 14	P 15	Cl 17	Ar 18	Ca 20	Ti 22	Cr 24	Mn 25	Fe 26	Ni 28	Cu 29	W 74	Pb 82
Aluminium	2.7						100													
Titanium	4.54												100							
Tungsten	19.3																		100	
Lead	11.34																			100
XC10	7.8		0.1												0.6	99.3				
Denal (WNICU)	16.8																7	2.5	90.5	
Stainless steel	7.8		0.02					1						18	2	68.98	10			
kapton	1.42	2.6362	69.113	7.327	20.924															
air	1.20E-03		0.0124	75.527	23.178						1.2827									
lung equivalent	0.3	8.33	60.08	2.73	23.04	4.8				1.02										
bone equivalent	1.8	3.73	30.11	1.08	33.55	2.09			7.83	0.04		21.57								
water	0.9982	11.11			88.89															
PMMA	1.19	8	60		32															

composition is given per mass

2.4 Note on geometrical details

All geometrical dimensions are given in mm except when otherwise mentioned. All geometrical details provided are as precise as possible. However, some aspects can be simplified, if necessary. For example, for a correct modelling of the beam it is not necessary to model the outer part of the flattening filter as it is not crossed by the beam (see Fig. 15).

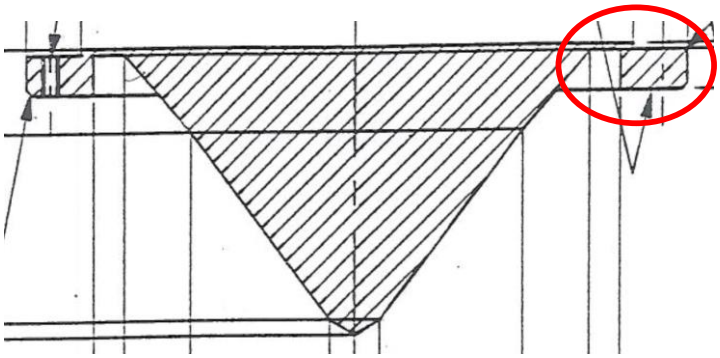

Fig. 15: Overview of the flattening filter at 12 MV

3. Data for performing Task1

The aim of Task1 is to model the head of the LINAC. To perform this task, it is necessary to adjust all the parameters the energy spectrum, the spot size and the shape of the electron beam impinging on the Titanium window. Adjustment should be performed by comparing simulated results with the experimentally measured beam profile and the percentage depth dose (PDD) curve for a 10x10 cm^2 field. These data are provided in the Table 3 "PDD-data in water" (see Annex 1) and in Table 4 "Profile-data in water" (see Annex 1). All the measurements were performed using a small volume ionization chamber (PTW 31002, 0.125 cm^3, PTW Freiburg, Germany).

A critical factor is the selection of the voxel size within the water phantom: the computational cost will be higher when small voxels are used. For the EURADOS WG6 Linac Action, it was proposed (but it was not mandatory) to use voxels with a size of 0.5x0.5x0.5 cm^3.

In order to compare the results and to adjust the requested parameters (energy spectrum etc), the gamma index should be used (see fig 17). This index takes into account both the relative shift in terms of intensity and in terms of position. To calculate the gamma index, it is necessary to consider two values, ΔD_{max} and Δx_{max}, around the experimental value. The values ΔD_{max} and Δx_{max} define the axes of an ellipsoid in which one can accept the calculated point. For each point of the data of the simulation to be compared (x_{ei}; D_{ei}), one calculates the gamma value in comparison with the measured reference point (x_{ri}; D_{ri}). The gamma index for (x_{ri}; D_{ri}) is the minimum value of all the gamma values. If the gamma index is less than or equal to unity, the comparison is accepted, if it is greater than unity, the point is rejected.

The calculation is repeated for each (x_{ri}; D_{ri}) value. The simulated data set is considered to be in agreement with the measured reference data set if for all data points (x_{ri}; D_{ri}) a gamma index equal or less than unity is obtained. If this is the case, the parameters used would be considered as optimum values.

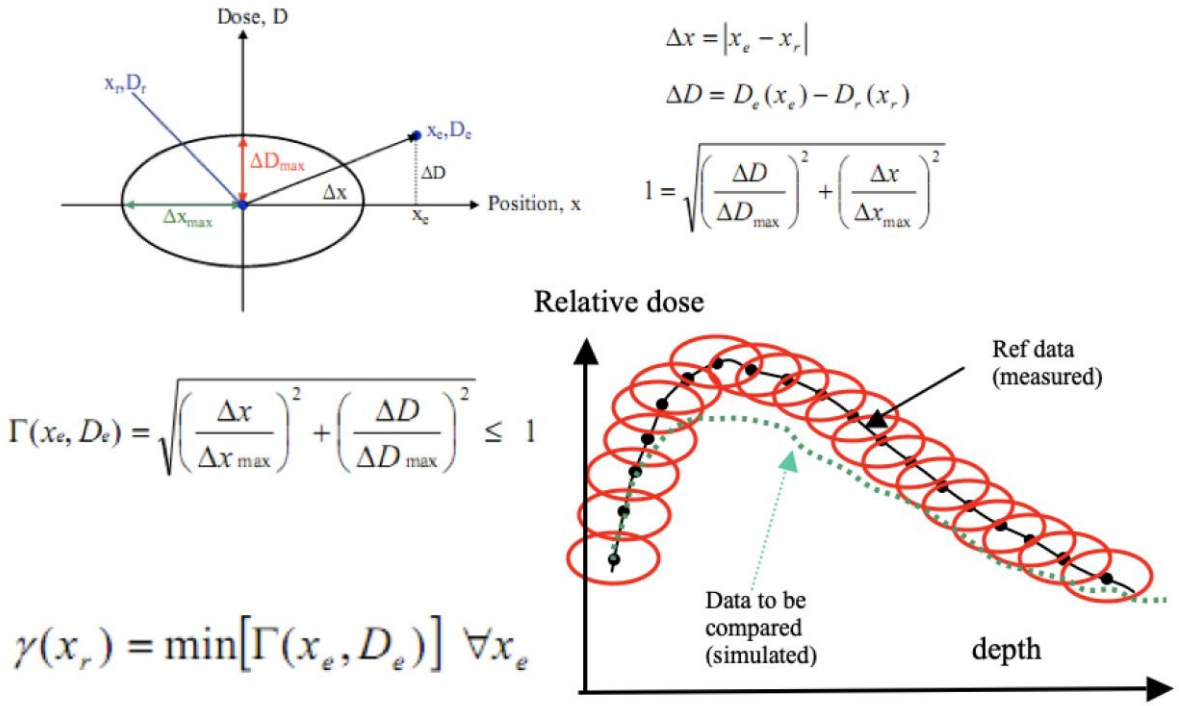

Fig. 16: Gamma index description.

The default values for the tolerances are 1 mm in position and 1 % in relative dose. It is highly recommended to use the same position of calculated and measured data so that x_e=x_r. Positions are provided in Tables 3 and 4 in Annex 1.

Once the optimum parameters of the electron beam have been established, a phase-space file (PSF) can be calculated to store particle information at the accelerator head output to avoid re-simulating the particle transport inside the head each time a different dosimetric phantom is used in the second task, which takes time. Note that creating the PSF file usually takes longer than simulating the energy deposition for the same number of initial particles.

4. Data for performing Task2

In the second task, the relative absorbed dose in water, including tissue equivalent heterogeneities, is to be calculated using the parameters of the source determined in the first task. As explained earlier, the depths for the calculation are expressed in cm. Nevertheless, for the comparison with the measured data (obtained in water only since the heterogeneities are made with solid phantoms), the comparison has to be performed with the depth expressed in g/cm^2 in order to be able to compare the results with the "only water" case. It is also highly recommended (see task 1) to use the same position for calculated and measured data, so that $x_e = x_r$.

Four configurations are proposed that include different solid inserts placed in the water phantom to mimic tissue equivalent heterogeneities: a) lung-equivalent tissue slab (phantom A); b) bone-equivalent tissue slab (phantom B); c) bone-equivalent and lung-equivalent tissue slabs (phantom C); d) two lung-equivalent tissue slabs (phantom D). Figs. 17 to 20 show photographs and schematic diagrams for the four configurations. The diagrams are not to scale.

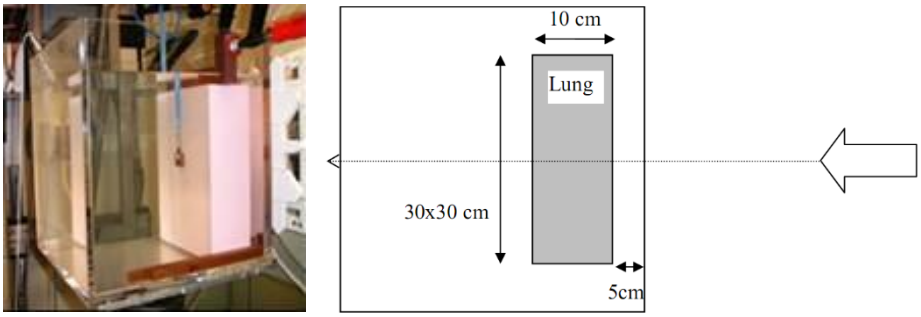

Fig. 17: Photograph and dimensioned drawing of dosimetric phantom A. This water phantom includes a lung tissue-equivalent cuboid slab. The reference dosimetric data for phantom A for measurements in water outside the lung slab are reported in Table 5 (see Annex 1).

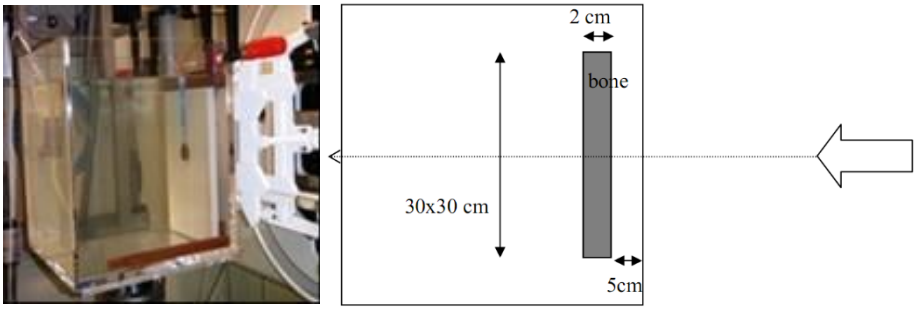

Fig. 18: Photograph and dimensioned drawing of dosimetric phantom B. This water phantom includes a bone tissue-equivalent cuboid slab. The reference dosimetric data for phantom B for measurements in water outside the bone slab are reported in Table 6 (see Annex 1).

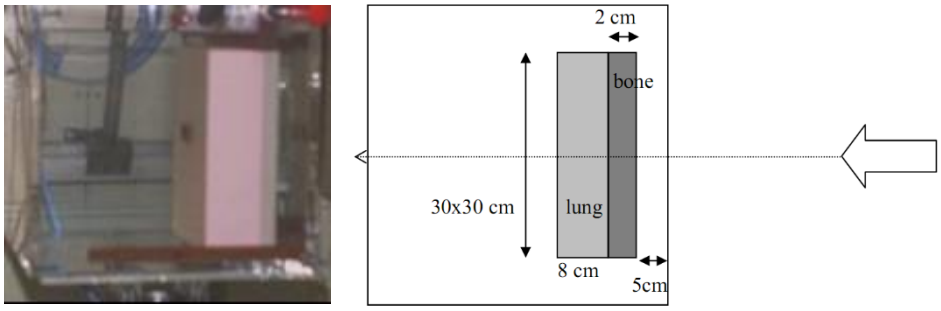

Fig. 19: Photograph and dimensioned drawing of dosimetric phantom C. This water phantom includes two cuboid slabs of bone and lung-equivalent material, respectively. The reference dosimetric data for phantom C for measurements in water outside the two slabs are reported in Table 7 (see Annex 1).

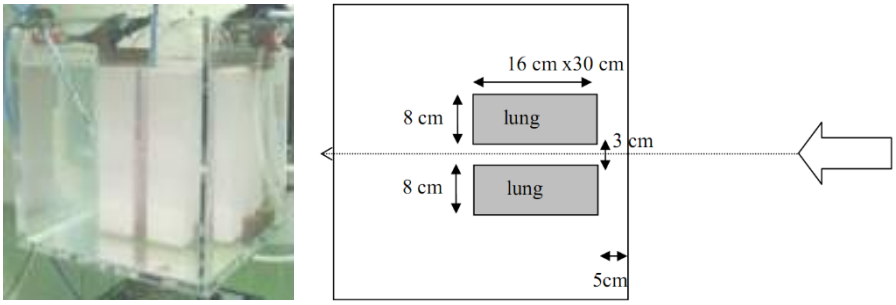

Fig. 20: Photograph and dimensioned drawing of dosimetric phantom D. This water phantom includes two cuboid slabs of lung-equivalent material. The reference dosimetric data for phantom D for measurements in water outside the two slabs are reported in Table 8 (see Annex 1).

In Figs. 17 to 20, the heterogeneities are placed at 5 cm from the front surface of the water phantom, such that the photon beam passed the 0.4 cm PMMA window and 4.6 cm of water before reaching them. The mass densities of the heterogeneities are 1.80 g/cm^3 for the bone material and 0.31 g/cm^3 for the lung material (Blazy *et al.*, 2006), the mass density of PMMA is 1.19 g/cm^3 and the water density 0.9982 g/cm^3.

The experimentally determined reference data used in the EURADOS LINAC Action for the different configurations were the following:

- for phantoms A), B) and C): PDD (Percentage Depth Dose) curves
- for phantom D) : lateral dose profiles (between -10 cm to +10 cm from the beam axis) at 22 and 25 cm depth.

To compare the results obtained by calculation with the experimental data given in Tables 5 to 8 in Annex 1, two important things have to be taken into account. The first is related to the fact that the depth in water is expressed in g/cm^2. The second aspect is related to the normalisation of the results.

- For cases A) to C) the results are given as the ratio of the dose per emitted-electron in the heterogeneous case to the dose per emitted-electron at 10 cm depth in the phantom on the central axis beam in the reference case (homogeneous water phantom, Task 1).
- for case D), the profiles are normalized such that on the central axis the PDD value is equal to the value measured in a homogenous water phantom (Task 1).

5. Conclusions from the Linac intercomparison action

In 2010 the Linac Action intercomparison exercise was proposed by the EURADOS Computational Dosimetry Working Group with the aim of comparing the results obtained when different MC code users apply different MC models to simulate a medical linear accelerator (linac), with models differing by MC code. The aim of the exercise was to identify critical aspects useful for MC users to build and calibrate a simulation and perform a dosimetric analysis. There were six responses to the exercise, coming from five different countries. Three results were obtained using different versions of BEAMnrc codes (Kawrakow 2000): BEAMnrc-DOSXYZnrc version 4.2.3.1 and BEAMnrc version 4. The other three were obtained with GEANT4 (version 9.2) (Agostinelli *et al.* 2003), MCNPX (version 2.5) (Pelowitz 2013) and TRIPOLI (version 4.7) (Brun *et al.* 2011).

Some significant differences have been observed, especially in presence of heterogeneities. Moreover, the results are critically dependent on the choice of the electron source parameters. The parameters for the initial electron beam chosen by the EURADOS intercomparison participants are shown in Table 2. The first column indicates an anonymised identification of the participant. The second column refers to the chosen electron energy distribution: the type of distribution and the characteristic parameters are indicated. The third column lists the characteristic of the electron beam spot. The definition of parameters for the electron beam spot is an important aspect of the MC simulation (Verhaegen *et al.* 2003; Fix *et al.* 2005). In this case different parameter settings were chosen by the participants, even for those using the same MC code.

Table 2. Electron source parameters chosen by participants.

Participant ID	Electron energy distribution	Electron beam spot
#1	Gaussian - Mean: 12.3 MeV FWHM: 0.290 MeV	Circular homogenous Diameter: 2 mm
#2	Gaussian - Mean: 11.7 MeV FWHM: 1.17 MeV	Circular Gaussian FWHM: 0.5 mm 0.5° divergence
#3	Monoenergetic 11.25 MeV	Point-like with complex angular distribution
#4	Gaussian - Mean: 12 MeV FWHM: N/A	Circular homogeneous Diameter: 0.8 mm
#5	Gaussian - Mean: 11.4 MeV FWHM: 0.5 MeV	Circular Gaussian FWHM: 1.7 mm
#6	Monoenergetic 11.5 MeV	Circular homogeneous Diameter: 1.5 mm

Figure 21 shows the percentage of the local dose differences between calculated and measured doses along the central axis in a water phantom for the six participants. The dashed lines represent the ±1% dose-difference region and the dotted line indicates the depth of build-up. Major disagreements between measurements and calculations occur in the build-up region. This is not a

surprise since in this region accurate ion chamber measurements are difficult to make, and calculations are very sensitive to the energy of the electron source (Keall *et al.* 2003). Differences between different participants could be explained by the influence of both the choice of the mean energy of the primary electrons and of the electron spot size. The dashed lines represent the ±1% dose-difference region and the dotted line indicates the depth of the build-up region.

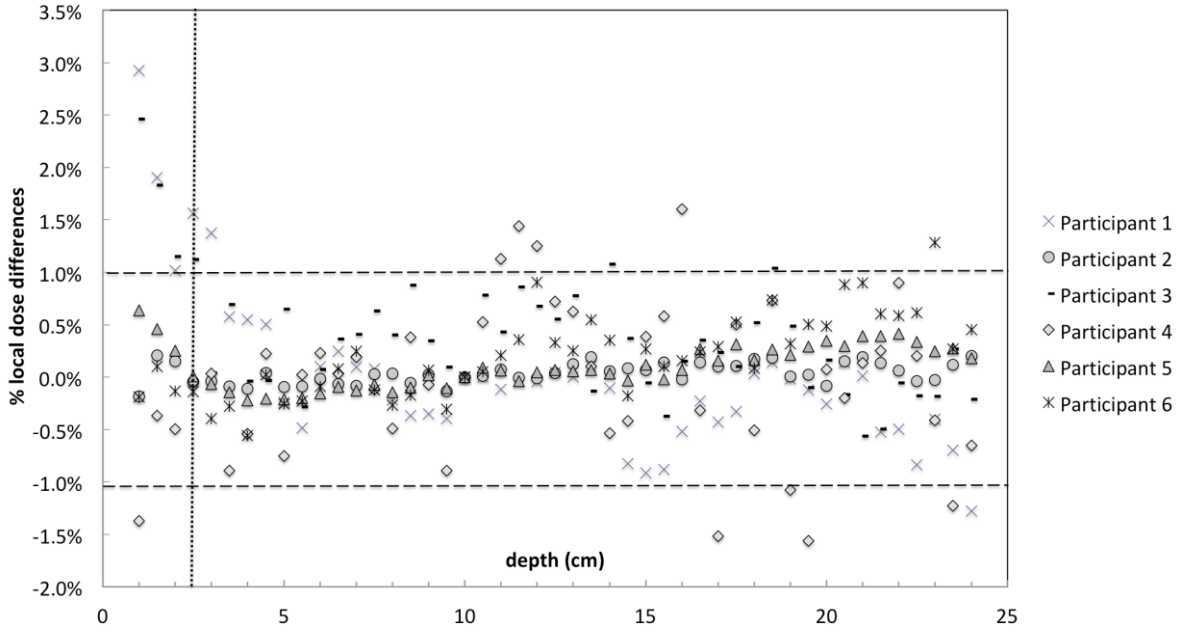

Fig. 21: Percentage of the local dose differences between calculated and measured doses (PDD) in a water phantom for the six participants. The dashed lines represent the ±1% dose-difference region and the dotted line indicates the depth of the build-up region.

Fig. 22 shows the percentage of the local dose differences between calculated and measured doses (PDD) in the case of Phantom-A (water phantom with a lung-equivalent material slab) as described in Section 4. The same participants that had discrepancies in the build-up zones for the water phantom (Fig. 21) show discrepancies in the same area (data are consistent, in this case). Dashed lines represent the ±1% dose-difference region, while the dotted line indicates the depth of the build-up region. All the results of the EURADOS Linac Action intercomparison have been published in an open access journal (Caccia *et al.* 2017).

The intercomparison allowed the six participants to identify some critical issues in MC modelling of a medical linear accelerator. It is clearly shown that there are different approaches for the determination of the initial electron beam characteristics, i.e. different geometrical model of the beam and different description of the electron source energy (even when using the same Monte Carlo code). Moreover, the results of dose distribution calculations in the presence of heterogeneities confirm the importance of proper electron source parameter choices: an inadequate model established using measurements in a water phantom inevitably leads to disagreements between calculations and measurements when adding heterogeneities.

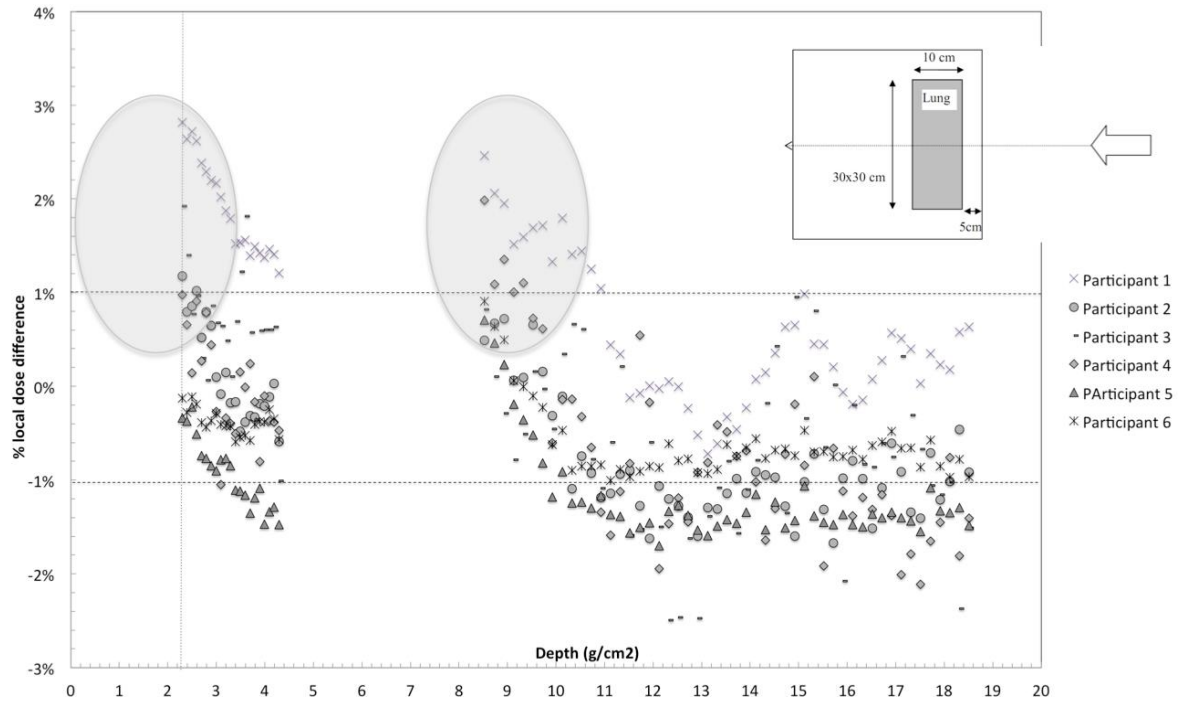

Fig. 22: Percentage of the local dose differences between calculated and measured doses (PDD) in the dosimetric Phantom-A (water phantom with a lung-equivalent material slab) for the six participants. The dashed lines represent the ±1% dose-difference region and the dotted vertical line indicates the depth of the build-up region.

6. References

Agostinelli S, Allison J, Amako KA, Apostolakis J, Arau- jo H, Arce P, Asai M, Axen D, Banerjee S, Barrand G.2003. GEANT4 – a simulation toolkit. Nucl Instrum Methods Phys Res, 506:250-303.

Blazy L, Baltes D, Bordy JM, Cutarella D, Delaunay F, Gouriou J, Leroy E, Ostrowsky A, Beaumont S. 2006. Comparison of PENELOPE Monte Carlo dose calculations with Fricke dosimeter and ionization chamber measurements in heterogeneous phantoms (18 MeV electron and 12 MV photon beams). Phys Med Biol; 51:5951-65. DOI: 10.1088/0031-9155/51/22/016

Brun E, Dumonteil E, Hugot FX, Huot N, Lee YK, Mal- vagi F, Mazzolo A, Petit O, Trama JC, Zoia A. Overview of TRIPOLI-4 version 7, Continuous-energy Monte Carlo Transport Code. In: International Congress on Advances in Nuclear Power Plants 2011. Proceedings. Nice: May 2-6, 2011. p. 1584-9.

Caccia B., Le Roy M., Blideanu V., Andenna C., Arun C., Czarnecki D., El Bardouni T., Gschwind R., Huot N., Martin E., Zink K., Zoubair M., Price R. and de Carlan L.2017. EURADOS intercomparison exercise on Monte Carlo modelling of a medical linear accelerator, Ann Ist Super Sanità, 53(4), 314-321. (https://annali-iss.eu/index.php/anna/article/view/581/0)

Depuydt T., Van Esch A., Huyskens D.P. 2002. A quantitative evaluation of IMRT dose distributions: refinement and clinical assessment of the gamma evaluation. Radiother Oncol, 62, 309-19.

Fix MK, Keall PJ, Siebers JV.2005. Photon-beam subsource sensitivity to the initial electron-beam parameters. Med Phys, 32:1164-75.

Kawrakow I.2000. Accurate condensed history Monte Carlo simulation of electron transport. I. EGSnrc, the new EGS4 version. Med Phys, 27:485-98.

Keall PJ, Siebers JV, Libby B, Mohan R. 2003. Determining the incident electron fluence for Monte Carlo-based photon treatment planning using a standard measured data set. Med Phys, 30:574-82.

Pelowitz DBE.2013. MCNP6TM User's Manual Version 1.0. LA-CP-13-00634.

Rogers D.W.O.2006. Fifty years of Monte Carlo simulations for medical physics. Phys Med Biol, 51:R287-R301.

Verhaegen F, Seuntjens J. 2003. Monte Carlo modelling of external radiotherapy photon beams. Phys Med Biol, 48:R107-64.

7. Annex 1: Listing of the data file contents

Table 3 PDD-data in water – Measured depth dose curve for a photon field of 10x10 cm^2 at 100 cm from the source; distance between source and phantom surface 90 cm; LINAC acceleration voltage 12 MV. All the experimental measurements were performed with a PTW 31002 ionization chamber (sensitive volume 0.125 cm^3). The third column gives the standard uncertainty that corresponds to a confidence interval of about 68% coverage.

Depth(cm)	Relative absorbed dose	absolute uncertainty at 1 sigma
1.0	1.1552	0.0046
1.5	1.2861	0.0051
2.0	1.3404	0.0054
2.5	1.3549	0.0054
3.0	1.3486	0.0054
3.5	1.3296	0.0053
4.0	1.3052	0.0052
4.5	1.2790	0.0051
5.0	1.2515	0.0050
5.5	1.2245	0.0049
6.0	1.1986	0.0048
6.5	1.1725	0.0047
7.0	1.1464	0.0046
7.5	1.1213	0.0045
8.0	1.0963	0.0044
8.5	1.0718	0.0043
9.0	1.0485	0.0042
9.5	1.0222	0.0041
10.0	**1.0000**	**0.0040**
10.5	0.9786	0.0039
11.0	0.9562	0.0038
11.5	0.9343	0.0037
12.0	0.9124	0.0036
12.5	0.8916	0.0036
13.0	0.8709	0.0035
13.5	0.8510	0.0034
14.0	0.8313	0.0033
14.5	0.8114	0.0032
15.0	0.7933	0.0032
15.5	0.7746	0.0031
16.0	0.7571	0.0030
16.5	0.7397	0.0030

Depth(cm)	Relative absorbed dose	absolute uncertainty at 1 sigma
17.0	0.7223	0.0029
17.5	0.7060	0.0028
18.0	0.6896	0.0028
18.5	0.6736	0.0027
19.0	0.6579	0.0026
19.5	0.6429	0.0026
20.0	0.6282	0.0025
20.5	0.6134	0.0025
21.0	0.5997	0.0024
21.5	0.5854	0.0023
22.0	0.5722	0.0023
22.5	0.5585	0.0022
23.0	0.5455	0.0022
23.5	0.5332	0.0021
24.0	0.5208	0.0021

Table 4 Profile-data in water – Measured lateral profile curve at 10 cm depth in water for a photon field of 10x10 cm^2 at 100 cm from the source; distance between source and phantom 90 cm; LINAC acceleration voltage 12 MV. All the experimental measurements were performed with a PTW 31002 ionization chamber (sensitive volume 0.125 cm^3). The third column gives the standard uncertainty that corresponds to a confidence interval of about 68% coverage.

Distance from central axis (cm)	Relative absorbed dose	absolute uncertainty at 1 sigma
-11.0	0.01800	0.00007
-10.5	0.02007	0.00008
-10.0	0.02288	0.00009
-9.5	0.02613	0.00010
-9.0	0.03011	0.00012
-8.5	0.03480	0.00014
-8.0	0.04035	0.00016
-7.5	0.04758	0.00019
-7.0	0.05675	0.00023
-6.5	0.07034	0.00028
-6.0	0.09687	0.00039
-5.5	0.17492	0.00070
-5.0	0.5284	0.0021
-4.5	0.8820	0.0035
-4.0	0.9609	0.0038
-3.5	0.9822	0.0039
-3.0	0.9904	0.0040
-2.5	0.9964	0.0040
-2.0	0.9960	0.0040
-1.5	1.0011	0.0040
-1.0	1.0031	0.0040
-0.5	1.0024	0.0040
0.0	**1.0000**	**0.0040**
0.5	1.0024	0.0040
1.0	1.0031	0.0040
1.5	1.0011	0.0040
2.0	0.9960	0.0040
2.5	0.9964	0.0040
3.0	0.9904	0.0040
3.5	0.9822	0.0039
4.0	0.9609	0.0038
4.5	0.8820	0.0035

Distance from central axis (cm)	Relative absorbed dose	absolute uncertainty at 1 sigma
5.0	0.5284	0.0021
5.5	0.17492	0.00070
6.0	0.09687	0.00039
6.5	0.07034	0.00028
7.0	0.05675	0.00023
7.5	0.04758	0.00019
8.0	0.04035	0.00016
8.5	0.03480	0.00014
9.0	0.03011	0.00012
9.5	0.02613	0.00010
10.0	0.02288	0.00009
10.5	0.02007	0.00008
11.0	0.01800	0.00007

Table 5 Reference_data_PhantomA – Depth dose curve for a photon field of 10x10 cm^2 at 100 cm from the source; distance between source and phantom surface 90 cm; LINAC acceleration voltage 12 MV. The reference dosimetric data for phantom A are reported for the water and not for the lung slab. The values in the fourth column are the expanded uncertainties for a confidence interval of about 95% coverage.

Material	Depth (g/cm^2)	Relative absorbed dose	absolute uncertainty at 2 sigmas
PMMA	0.00 - 0.48	density 1.19 g/cm^3, no measurement data available	
WATER	2.30	1.3522	0.0097
	2.40	1.3514	0.0097
	2.50	1.3549	0.0098
	2.60	1.3545	0.0098
	2.70	1.3515	0.0097
	2.80	1.3494	0.0097
	2.89	1.3480	0.0097
	2.99	1.3461	0.0097
	3.09	1.3413	0.0097
	3.19	1.3377	0.0096
	3.29	1.3340	0.0096
	3.39	1.3278	0.0096
	3.49	1.3239	0.0095
	3.59	1.3191	0.0095
	3.69	1.3128	0.0095
	3.79	1.3091	0.0094
	3.89	1.3034	0.0094
	3.99	1.2976	0.0093
	4.09	1.2939	0.0093
	4.19	1.2879	0.0093
	4.29	1.2806	0.0092
LUNG	5.07 – 8.17	density 0.31 g/cm^3, no measurement data available	
WATER	8.53	0.8931	0.0064
	8.73	0.8874	0.0064
	8.93	0.8811	0.0063
	9.13	0.8715	0.0063
	9.33	0.8650	0.0062
	9.53	0.8583	0.0062
	9.73	0.8513	0.0061
	9.93	0.8421	0.0061
	10.13	0.8375	0.0060
	10.33	0.8279	0.0060
	10.53	0.8221	0.0059

Material	Depth (g/cm^2)	Relative absorbed dose	absolute uncertainty at 2 sigmas
WATER	10.73	0.8157	0.0059
	10.93	0.8093	0.0058
	11.13	0.8013	0.0058
	11.33	0.7955	0.0057
	11.52	0.7880	0.0057
	11.72	0.7816	0.0056
	11.92	0.7752	0.0056
	12.12	0.7683	0.0055
	12.32	0.7635	0.0055
	12.52	0.7555	0.0054
	12.72	0.7491	0.0054
	12.92	0.7417	0.0053
	13.12	0.7353	0.0053
	13.32	0.7294	0.0053
	13.52	0.7251	0.0052
	13.72	0.7182	0.0052
	13.92	0.7128	0.0051
	14.12	0.7075	0.0051
	14.32	0.7001	0.0050
	14.52	0.6947	0.0050
	14.72	0.6889	0.0050
	14.92	0.6824	0.0049
	15.12	0.6783	0.0049
	15.32	0.6707	0.0048
	15.52	0.6648	0.0048
	15.72	0.6585	0.0047
	15.92	0.6526	0.0047
	16.12	0.6472	0.0047
	16.32	0.6408	0.0046
	16.52	0.6360	0.0046
	16.72	0.6307	0.0045
	16.92	0.6259	0.0045
	17.11	0.6194	0.0045
	17.31	0.6141	0.0044
	17.51	0.6077	0.0044
	17.71	0.6044	0.0044
	17.91	0.5977	0.0043
	18.11	0.5920	0.0043

Material	Depth (g/cm^2)	Relative absorbed dose	absolute uncertainty at 2 sigmas
WATER	18.31	0.5880	0.0042
	18.51	0.5816	0.0042

Table 6 Reference_data_PhantomB – Depth dose curve for a photon field of 10x10 cm^2 at 100 cm from the source; distance between source and phantom surface 90 cm; LINAC acceleration voltage 12 MV. The reference dosimetric data for the phantom B are reported for the water and not for the bone slab. The values in the fourth column are the expanded uncertainties for a confidence interval of about 95% coverage.

Material	Depth (g/cm^2)	Relative absorbed dose	Absolute uncertainty at 2 sigmas
PMMA	0.00 - 0.48	density 1.19 g/cm^3, no measurement data available	
WATER	2.30	1.3608	0.0098
	2.40	1.3628	0.0098
	2.50	1.3620	0.0098
	2.60	1.3624	0.0098
	2.70	1.3606	0.0098
	2.80	1.3604	0.0098
	2.89	1.3571	0.0098
	2.99	1.3531	0.0097
	3.09	1.3509	0.0097
	3.19	1.3473	0.0097
	3.29	1.3425	0.0097
	3.39	1.3386	0.0096
	3.49	1.3349	0.0096
	3.59	1.3292	0.0096
	3.69	1.3251	0.0095
	3.79	1.3203	0.0095
	3.89	1.3137	0.0095
	3.99	1.3100	0.0094
	4.09	1.3048	0.0094
	4.19	1.3003	0.0094
	4.29	1.2948	0.0093
BONE	5.07 - 8.67	density 1.80 g/cm^3, no measurement data available	
WATER	9.06	1.0874	0.0078
	9.25	1.0793	0.0078
	9.45	1.0690	0.0077
	9.65	1.0582	0.0076
	9.85	1.0473	0.0075
	10.05	1.0391	0.0075
	10.25	1.0292	0.0074
	10.45	1.0180	0.0073
	10.65	1.0088	0.0073
	10.85	1.0002	0.0072
	11.05	0.9890	0.0071

Material	Depth (g/cm^2)	Relative absorbed dose	Absolute uncertainty at 2 sigmas
WATER	11.25	0.9813	0.0071
	11.45	0.9704	0.0070
	11.65	0.9620	0.0069
	11.85	0.9509	0.0068
	12.05	0.9438	0.0068
	12.25	0.9348	0.0067
	12.45	0.9258	0.0067
	12.65	0.9178	0.0066
	12.85	0.9089	0.0065
	13.05	0.8986	0.0065
	13.25	0.8913	0.0064
	13.45	0.8817	0.0063
	13.65	0.8739	0.0063
	13.85	0.8634	0.0062
	14.05	0.8560	0.0062
	14.25	0.8496	0.0061
	14.45	0.8410	0.0061
	14.65	0.8326	0.0060
	14.85	0.8256	0.0059
	15.04	0.8159	0.0059
	15.24	0.8101	0.0058
	15.44	0.8010	0.0058
	15.64	0.7936	0.0057
	15.84	0.7861	0.0057
	16.04	0.7786	0.0056
	16.24	0.7706	0.0055
	16.44	0.7626	0.0055
	16.64	0.7541	0.0054
	16.84	0.7477	0.0054
	17.04	0.7434	0.0054
	17.24	0.7343	0.0053
	17.44	0.7289	0.0052
	17.64	0.7195	0.0052
	17.84	0.7134	0.0051
	18.04	0.7071	0.0051
	18.24	0.7001	0.0050
	18.44	0.6928	0.0050
	18.64	0.6874	0.0049

Material	Depth (g/cm^2)	Relative absorbed dose	Absolute uncertainty at 2 sigmas
WATER	18.84	0.6800	0.0049
	19.04	0.6730	0.0048
	19.24	0.6666	0.0048
	19.44	0.6609	0.0048
	19.64	0.6535	0.0047
	19.84	0.6470	0.0047
	20.04	0.6432	0.0046
	20.24	0.6362	0.0046
	20.44	0.6295	0.0045
	20.63	0.6234	0.0045
	20.83	0.6172	0.0044
	21.03	0.6115	0.0044
	21.23	0.6061	0.0044
	21.43	0.5996	0.0043
	21.63	0.5948	0.0043
	21.83	0.5887	0.0042
	22.03	0.5835	0.0042
	22.23	0.5784	0.0042
	22.43	0.5732	0.0041
	22.63	0.5672	0.0041
	22.83	0.5639	0.0041
	23.03	0.5559	0.0040
	23.23	0.5530	0.0040
	23.43	0.5474	0.0039
	23.63	0.5407	0.0039
	23.83	0.5367	0.0039
	24.03	0.5314	0.0038

Table 7 Reference_data_PhantomC – Depth dose curve for a photon field of 10x10 cm^2 at 100 cm from the source; distance between source and phantom surface 90 cm; LINAC acceleration voltage 12 MV. The reference dosimetric data for phantom C are reported for the water and not for the bone and lung slabs. The values in the fourth column are the expanded uncertainties for a confidence interval of about 95% coverage.

Material	Depth (g/cm^2)	Relative absorbed dose	Absolute uncertainty at 2 sigmas
PMMA	0.00 - 0.48	density 1.19 g/cm^3, no measurement data available	
WATER	2.30	1.3488	0.0097
	2.40	1.3522	0.0097
	2.50	1.3519	0.0097
	2.60	1.3504	0.0097
	2.70	1.3505	0.0097
	2.80	1.3498	0.0097
	2.89	1.3447	0.0097
	2.99	1.3440	0.0097
	3.09	1.3409	0.0097
	3.19	1.3367	0.0096
	3.29	1.3341	0.0096
	3.39	1.3295	0.0096
	3.49	1.3244	0.0095
	3.59	1.3186	0.0095
	3.69	1.3145	0.0095
	3.79	1.3098	0.0094
	3.89	1.3064	0.0094
	3.99	1.3003	0.0094
	4.09	1.2940	0.0093
	4.19	1.2898	0.0093
	4.29	1.2838	0.0092
BONE	5.07 – 8.67	density 1.80 g/cm^3, no measurement data available	
LUNG	8.67-11.15	density 0.31 g/cm^3, no measurement data available	
WATER	11.61	0.8284	0.0060
	11.81	0.8216	0.0059
	12.01	0.8142	0.0059
	12.21	0.8072	0.0058
	12.41	0.8008	0.0058
	12.61	0.7934	0.0057
	12.81	0.7860	0.0057
	13.01	0.7801	0.0056
	13.21	0.7743	0.0056
	13.41	0.7674	0.0055

Material	Depth (g/cm^2)	Relative absorbed dose	Absolute uncertainty at 2 sigmas
WATER	13.61	0.7599	0.0055
	13.81	0.7535	0.0054
	14.01	0.7471	0.0054
	14.21	0.7413	0.0053
	14.41	0.7343	0.0053
	14.60	0.7279	0.0052
	14.80	0.7215	0.0052
	15.00	0.7157	0.0052
	15.20	0.7093	0.0051
	15.40	0.7029	0.0051
	15.60	0.6976	0.0050
	15.80	0.6906	0.0050
	16.00	0.6842	0.0049
	16.20	0.6790	0.0049
	16.40	0.6731	0.0048
	16.60	0.6665	0.0048
	16.80	0.6623	0.0048
	17.00	0.6560	0.0047
	17.20	0.6482	0.0047
	17.40	0.6425	0.0046
	17.60	0.6380	0.0046
	17.80	0.6312	0.0045
	18.00	0.6261	0.0045
	18.20	0.6212	0.0045
	18.40	0.6155	0.0044
	18.60	0.6105	0.0044
	18.80	0.6048	0.0044
	19.00	0.5992	0.0043
	19.20	0.5930	0.0043
	19.40	0.5882	0.0042
	19.60	0.5833	0.0042
	19.80	0.5773	0.0042
	20.00	0.5726	0.0041
	20.19	0.5674	0.0041
	20.39	0.5626	0.0041
	20.59	0.5557	0.0040
	20.79	0.5514	0.0040
	20.99	0.5473	0.0039

Material	Depth (g/cm^2)	Relative absorbed dose	Absolute uncertainty at 2 sigmas
WATER	21.19	0.5425	0.0039
	21.39	0.5369	0.0039
	21.59	0.5342	0.0038

Table 8 Reference_data_PhantomD_z22 and PhantomD_z25 – Profile curves at 22 cm and 25 cm depth in water for a photon field of 10x10 cm² at 100 cm from the source; distance between source and phantom surface 90 cm; LINAC acceleration voltage 12 MV. The values in columns three and five are expanded uncertainties for a confidence interval of about 95% coverage.

Distance from central axis (cm)	22 cm depth in water		25 cm depth in water	
	Relative absorbed dose	Absolute uncertainty at 2 sigmas	Relative absorbed dose	Absolute uncertainty at 2 sigmas
-8.60	0.0416	0.0003	0.0384	0.0003
-8.40	0.0446	0.0003	0.0397	0.0003
-8.20	0.0467	0.0003	0.0421	0.0003
-8.00	0.0501	0.0004	0.0450	0.0003
-7.80	0.0533	0.0004	0.0472	0.0003
-7.60	0.0565	0.0004	0.0493	0.0004
-7.40	0.0600	0.0004	0.0522	0.0004
-7.20	0.0661	0.0005	0.0551	0.0004
-7.00	0.0724	0.0005	0.0614	0.0004
-6.80	0.0793	0.0006	0.0691	0.0005
-6.60	0.0897	0.0006	0.0784	0.0006
-6.40	0.1045	0.0008	0.0966	0.0007
-6.20	0.1258	0.0009	0.1284	0.0009
-6.00	0.1679	0.0012	0.1931	0.0014
-5.80	0.2460	0.0018	0.2918	0.0021
-5.60	0.3642	0.0026	0.4077	0.0029
-5.40	0.4945	0.0036	0.5065	0.0036
-5.20	0.5964	0.0043	0.5738	0.0041
-5.00	0.6547	0.0047	0.6082	0.0044
-4.80	0.6849	0.0049	0.6260	0.0045
-4.60	0.7015	0.0051	0.6362	0.0046
-4.40	0.7126	0.0051	0.6430	0.0046
-4.20	0.7211	0.0052	0.6462	0.0047
-4.00	0.7264	0.0052	0.6502	0.0047
-3.80	0.7309	0.0053	0.6522	0.0047
-3.60	0.7343	0.0053	0.6523	0.0047
-3.40	0.7372	0.0053	0.6538	0.0047
-3.20	0.7383	0.0053	0.6549	0.0047
-3.00	0.7391	0.0053	0.6542	0.0047
-2.80	0.7386	0.0053	0.6528	0.0047
-2.60	0.7377	0.0053	0.6509	0.0047
-2.40	0.7346	0.0053	0.6470	0.0047

Distance from central axis (cm)	22 cm depth in water		25 cm depth in water	
	Relative absorbed dose	Absolute uncertainty at 2 sigmas	Relative absorbed dose	Absolute uncertainty at 2 sigmas
-2.20	0.7285	0.0052	0.6401	0.0046
-2.00	0.7133	0.0051	0.6222	0.0045
-1.80	0.6768	0.0049	0.5866	0.0042
-1.60	0.6267	0.0045	0.5430	0.0039
-1.40	0.5857	0.0042	0.5096	0.0037
-1.20	0.5627	0.0041	0.4941	0.0036
-1.00	0.5528	0.0040	0.4863	0.0035
-0.80	0.5500	0.0040	0.4835	0.0035
-0.60	0.5493	0.0040	0.4820	0.0035
-0.40	0.5479	0.0039	0.4798	0.0035
-0.20	0.5467	0.0039	0.4782	0.0034
0.00	0.5455	0.0039	0.4772	0.0034
0.20	0.5467	0.0039	0.4782	0.0034
0.40	0.5479	0.0039	0.4798	0.0035
0.60	0.5493	0.0040	0.4820	0.0035
0.80	0.5500	0.0040	0.4835	0.0035
1.00	0.5528	0.0040	0.4863	0.0035
1.20	0.5627	0.0041	0.4941	0.0036
1.40	0.5857	0.0042	0.5096	0.0037
1.60	0.6267	0.0045	0.5430	0.0039
1.80	0.6768	0.0049	0.5866	0.0042
2.00	0.7133	0.0051	0.6222	0.0045
2.20	0.7285	0.0052	0.6401	0.0046
2.40	0.7346	0.0053	0.6470	0.0047
2.60	0.7377	0.0053	0.6509	0.0047
2.80	0.7386	0.0053	0.6528	0.0047
3.00	0.7391	0.0053	0.6542	0.0047
3.20	0.7383	0.0053	0.6549	0.0047
3.40	0.7372	0.0053	0.6538	0.0047
3.60	0.7343	0.0053	0.6523	0.0047
3.80	0.7309	0.0053	0.6522	0.0047
4.00	0.7264	0.0052	0.6502	0.0047
4.20	0.7211	0.0052	0.6462	0.0047
4.40	0.7126	0.0051	0.6430	0.0046
4.60	0.7015	0.0051	0.6362	0.0046
4.80	0.6849	0.0049	0.6260	0.0045

Distance from central axis (cm)	22 cm depth in water		25 cm depth in water	
	Relative absorbed dose	Absolute uncertainty at 2 sigmas	Relative absorbed dose	Absolute uncertainty at 2 sigmas
5.00	0.6547	0.0047	0.6082	0.0044
5.20	0.5964	0.0043	0.5738	0.0041
5.40	0.4945	0.0036	0.5065	0.0036
5.60	0.3642	0.0026	0.4077	0.0029
5.80	0.2460	0.0018	0.2918	0.0021
6.00	0.1679	0.0012	0.1931	0.0014
6.20	0.1258	0.0009	0.1284	0.0009
6.40	0.1045	0.0008	0.0966	0.0007
6.60	0.0897	0.0006	0.0784	0.0006
6.80	0.0793	0.0006	0.0691	0.0005
7.00	0.0724	0.0005	0.0614	0.0004
7.20	0.0661	0.0005	0.0551	0.0004
7.40	0.0600	0.0004	0.0522	0.0004
7.60	0.0565	0.0004	0.0493	0.0004
7.80	0.0533	0.0004	0.0472	0.0003
8.00	0.0501	0.0004	0.0450	0.0003
8.20	0.0467	0.0003	0.0421	0.0003
8.40	0.0446	0.0003	0.0397	0.0003
8.60	0.0416	0.0003	0.0384	0.0003